

CRANFIELD UNIVERSITY

Jose Manuel Amieva Llavona

Development and assessment of a novel hydro turbine for small
scale applications

School of Water, Energy and Environment
Renewable Energy Engineering

MSc
Academic Year: 2017 - 2018

Supervisor: Dr. Ali Nabavi
September 2018

CRANFIELD UNIVERSITY

School of Water, Energy and Environment
Renewable Energy Engineering

MSc

Academic Year 2017 - 2018

Jose Manuel Amieva Llavona

Development and assessment of a novel hydro turbine for small
scale applications

Supervisor: Dr Ali Nabavi
September 2018

This thesis is submitted in partial fulfilment of the requirements for
the degree of Master of Science.

© Cranfield University 2018. All rights reserved. No part of this
publication may be reproduced without the written permission of the
copyright owner.

ABSTRACT

Small-scale hydropower is one of the most efficient energy technologies for rural electrification both in less developed and developed countries. This technology can be considered where the large-scale opportunities either have been exploited already, or not classified as environmentally benign anymore. This report aims to propose and study a novel design of a water turbine for small-scale applications. A series of 3-D numerical models were developed to evaluate the feasibility of the proposed concepts, using Ansys® Fluent v. 18.2. The model is validated with developed analytical solutions. Even if the scope of the project is to formulate the concept of the turbine and validate the CFD model, simulations with different arrangements in which some improving measures with respect to the first design have been carried out. It was found that a C_p of $4.27E-02$ can be achieved in the best scenario simulated. However, predictions of the C_p showed that the C_p could be increased up to $1.9E-01$.

Keywords:

Renewable energy, Hydro power, Vertical axis water turbine, Drag-type, CFD, Turbine design.

ACKNOWLEDGEMENTS

First things first, I would like to express my sincerest gratitude to Dr Ali Nabavi for giving me the opportunity to do this thesis. In spite of the matter of this thesis not being on his research lines, he trusted on the idea and brought me the opportunity to develop it. Besides, I have to thank his unconditional and continuous support, guidance and insight throughout this project.

Secondly, I would like to thank to any person I have share good time with here in Cranfield. Since, despite the hard work done, the time flew this year "*en todos los trabajos se fuma*". Thus, special thanks to "los chavales", "real climbers", "las ratas" and the Cranfield basketball team. However, on top of these I have to do a special mention to my new family of B3F3 which gave me support every single day of this year. Within this family my special thanks to our little portuguese girl Marta who made of this thesis something readable.

Last but not least, I want to grate my family for the support received during my whole life. Particularly, my parents, my siblings and my brother in law, they have always trusted me and supported me to pursue my dreams and ambitions whatever it takes. There is no way I would be where I stand today if it were not for them.

I would not like to finish these acknowledgements without grating Jose Manuel Llavona Llavona, my grandfather who did his utmost to take care about his family always. He looked after myself, my whole life transmitting me, principles and made of me the person who I am today and somehow he is still doing it.

TABLE OF CONTENTS

ABSTRACT	i
ACKNOWLEDGEMENTS.....	ii
LIST OF FIGURES.....	v
LIST OF TABLES	vii
LIST OF EQUATIONS.....	viii
LIST OF ABBREVIATIONS	ix
1 Introduction.....	1
1.1 Aims and objectives	1
1.2 Layout of the report.....	2
2 Literature review.....	3
2.1 Water current turbines	3
2.1.1 Types of water turbines	3
2.1.2 Turbines characterisation	8
2.1.3 Drag-Based turbines	10
2.2 Computational Fluid Dynamics	11
3 Proposed concept	13
4 Methods.....	17
4.1 CFD model.....	17
4.1.1 Geometry	17
4.1.2 Mesh	19
4.1.3 Set up of the simulation.....	21
4.2 Analytical solution	26
4.3 Sensitive analysis and validation	29
4.4 Finding the optimal Tip Speed Ratio	29
4.5 Influence of the inertia around the shaft.....	30
4.6 New configurations	30
5 Results and Discussion	32
5.1 Sensitive analysis	33
5.2 Validation results.....	35
5.3 Optimal tip speed ratio	37
5.4 Influence of inertia around the shaft.....	37
5.5 New configuration results.....	41
5.5.1 Two pairs of blades	41
5.5.2 Four pairs of blades.....	42
5.5.3 Shape of the of the blades	44
6 Conclusions.....	46
7 Future work	48
REFERENCES.....	50
APPENDICES	54

LIST OF FIGURES

Figure 1. Water wheels, overshoot, undershoot and breast wheels respectively [6].	4
Figure 2. Head vs flow ranges of micro-hydro turbines [6].	5
Figure 3. Water stream turbines, Axial Flow Water Turbine, and Cross Flow Water Turbine from left to right respectively [10].	6
Figure 4. Vertical turbines, Savonius rotor, Darrieus rotor and H-Darrieus rotor respectively [12].	7
Figure 5. Power coefficients of rotors with different TSR [15].	9
Figure 6. Schematic drawing showing the drag forces exert on two blade Savonius [16].	10
Figure 7. Kawamura simulation, time history of the torque coefficient vs the angle of rotation (Tip speed ratio is 0.25) [21].	12
Figure 8. Wireframe view and solid model of the Aeolum Harvester design and its mesh for the simulations [20].	12
Figure 9. Diagram of velocities and drag forces of the turbine.	13
Figure 10. Sequence of half lap of the turbine represented with the velocity of the flow in the plane xz.	14
Figure 11. Render of a possible position of the turbine in a channel.	15
Figure 12. Velocity profile of a random channel of water [23].	15
Figure 13. Render of the prototype proposed with the name of each part.	16
Figure 14. Wireframe view of the entire domain. The dimensions are in mm.	17
Figure 15. Wireframe view of the entire domain showing the control volume used to calculate the velocity of the flow.	18
Figure 16. Domain, mesh and named parts of the geometry.	20
Figure 17. Different approaches for the model, (a) beginning of the simulation t=0 s, (b) t=2 s inner mesh moving, (c) t=2 s outer domain moving.	23
Figure 18. Velocities diagram of the blades.	26
Figure 19. Diagram of the pitch force and velocities. Where the forces are in red and velocities in blue.	28
Figure 20. Sequence of one lap of the turbine represented with the velocity of the flow in the plane xz.	32
Figure 21. Torque extracted from the turbine and its pitch position along six laps.	33

Figure 22. Sensitive analysis for the simulation rotating at 1 rad/s.....	34
Figure 23. Comparison between the analytical results and the Ansys® Fluent v. 18.2 results of the angle of pitch.....	35
Figure 24. Comparison between the two-analytical approach and the reference simulation.	36
Figure 25. Power coefficient as function of the Tip Speed Ratio.	37
Figure 26. Influence of inertia on the average Power Coefficient.	38
Figure 27. The effect of the inertia on: the C_p (figure on top) and on the angle of the pitch figure on the bottom. Both graphs are along one lap and during the same lap of the simulation, the fourth.....	40
Figure 28. Two pair of blades configuration.	41
Figure 29. Pitch angle and torque generated by 2 pair of blades.	42
Figure 30. Design and arrangement of the turbine with four pairs of blades. ...	43
Figure 31. Four pair of blades colour contours from simulation.....	43
Figure 32. Optimization of the shape of blades with the analytical model.	44
Figure 33. Holes manufactured on the blades in order to reduce the inertia. ...	57
Figure 34. Blades split in different plates in order to reduce the inertia.	57
Figure 35. Twisted blades in order to increase the force on the blades.	58

LIST OF TABLES

Table 1. Results of the sensitive analysis.....	34
Table 2. Result from the inertia analysis.	38

LIST OF SYMBOLS

Symbol	Description	Unit
A	projected area	m^2
ρ	density	kg/m^3
B_L	blockage effect	---
C_p	power coefficient	---
F_D	drag force	N
C_d	drag coefficient	---
R	radius	m
w	angular velocity	rad/s
t	time	s
u	flow velocity	m/s
μ	dynamic viscosity	kg/m·s
C_m	moment coefficient	---
λ	tip speed ratio	---
β	pitch angle	$^\circ$
I_z	inertia around z	$kg \cdot m^2$
w_z	pitch velocity	rad/s
α_z	pitch acceleration	rad/s ²

LIST OF ABBREVIATIONS

CFD	Computational Fluid Dynamics
AFWT	Axial Flow Water Turbines
CFWT	Cross Flow Water Turbine
TSR	Tip Speed Ratio
RANS	Reynolds Averaged Navier Stokes
VOF	Volume of Fluid
UDF	User Defined Function

1 Introduction

Simulated by recent technological developments and increasing concern over the sustainability and environmental impact of conventional fuel usage, the prospect of producing clean sustainable power in substantial quantities from renewable energy sources arouses interest around the world [1].

Hence, the provision of sustainable energy supplies is one of the major issues that today civilization is facing. Renewable energy examines both the physical and technological aspects behind deriving power from natural resources [2]. In an attempt of develop alternative to the conventional devices to extract this energy from natural resources. This thesis proposed a new concept of river current energy conversion system.

The increasing reports on technical and economic feasibility on the last decades about river current turbines have proven to reduce the cost-effective of electricity [3]. Thus, the important of these devices are taking more interest in the renewable energy industry.

1.1 Aims and objectives

As aforementioned this report aims to propose and study a new concept of hydro turbine for small-scale applications. This turbine attempts to irrput in the market based on two key factors:

- **Simplicity**, since typically turbines tend to have complex designs in order to be as efficient as possible. This new concept proposed has a simple design in order to have a simple manufacturing process to make a cheaper turbine.
- **Low environmental impact**, the second key factor of the design is to hold the environment and the visual impact a lower as possible.

Thus, the main objectives of the project are:

- Formulate the concept of the turbine and develop a Computational Fluid Dynamic (CFD) model in Ansys® Fluent.
- Study the convergence and the way to validate the model proposed.

- Prove the concept as capable of energy production.

1.2 Layout of the report

Following to this chapter in this work it is possible to find the literature review as chapter two. There all the theoretical background needed to understand and follow the present thesis.

Then The model proposed is presented on the chapter three, in order to explain the concept before going to the methodical followed during the project. Thus, the following chapter is methods where all the process of the study done during the work is explained. The results of this studied is presented and discussed on the chapter five, "Results and Discussion"

To conclude this work in chapter six and seven the conclusion of the work and the future work are presented. After this main body it is possible to find the references and the appendices.

2 Literature review

The following chapter contains the information needed to understand and follow the present work. Thus, it is divided in two parts mainly. The first part is based on the types of turbines that have been developed and their applications. The second part focuses on conducted numerical works and how CFD modelling can be used as a reliable tool to assess the design of a new hydro-turbine.

2.1 Water current turbines

With regards to of hydro power, the most common way to extract energy is building any sort of dam or barrage that creates a static head of water a river or channel. This technology provides a reliable and predictable energy supply which is available 24 hours per day. However, the impact on rivers and the capital cost of the dams or barrages are quite high. Thus, in spite of the reliability and predictability of this technology, alternative technologies have been proposed to address those drawbacks [4].

This work focuses more on small-scale applications of hydro turbines or pico-hydro turbines, which has been demonstrated as reliable and useful source for electricity production [5]. This source of energy has been identified as decentralized and renewable power, with high potential for rural electrifications as well as municipal waterways and irrigation systems [2].

2.1.1 Types of water turbines

The fact that any physical configuration that produces an asymmetric force about its axis on any kind of current would generate torque about its axis, has resulted in many different types of water turbines. In general, they can be classified in, water-head turbines, and water stream turbines [2].

2.1.1.1 The water-head turbines

These devices need a dam or a head water channel to feed the turbine. Basically, these turbines rotate by transforming the potential energy of the water into kinetic energy. The water-head turbines can also classified in two groups, namely, waterwheels, and water turbines [6].

- The firsts and more primitive devices are waterwheels. Waterwheels are not so relevant to the modern hydro-electric power generation, therefore, they are not commonly used in modern hydro-electric plants in the industrialised countries. However, they are particularly useful in remote areas and developing countries to pump water and produce electricity. The most common waterwheels are the undershot, the overshoot and the high-breast wheels, Figure 1[6].

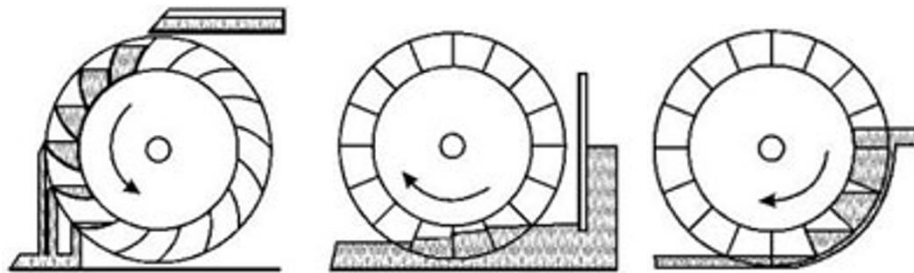


Figure 1. Water wheels, overshoot, undershoot and breast wheels respectively [6].

The major problems of these turbines are: (1) their size which are between one and three times larger than the potential head of the current; and (2) the low angular velocity that they have as output. Their efficiency is between 35% and 85% in the best case which is achieved in the overshoot water wheel [7].

- Water turbines, due to their rapid response to the demand of electricity and the high efficiency, account for a great portion of the energy in the grid in developed countries. There are basically four different types of turbines, the Pelton wheel, the Francis turbine, crossflow turbines and axial-flow turbines (i.e. Deriaz and Kaplan). The suitability of these turbines of each particular application is determined based on the head and the discharge of the flow available, Figure 2.

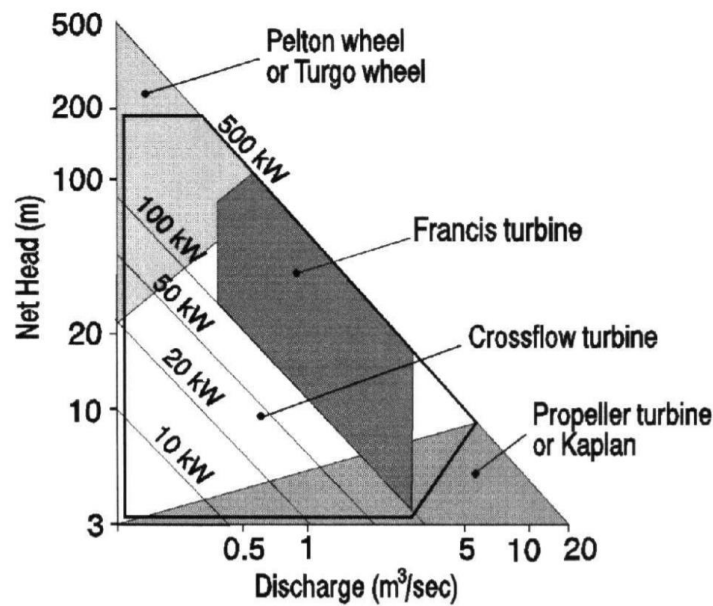


Figure 2. Head vs flow ranges of micro-hydro turbines [6].

These configurations offer controllable, predictable and high efficiency energy. On the other hand, they require big investments and modifications on the basins of the river or/and constructions of dams. The constructions of dams were an emerging technology during the twentieth century for the management of water resources and production of energy. Therefore, most of the major places where this technology is suitable are already being exploited. However, in other locations, the environmental cost of these structures is apparent and unacceptable. In fact, they break down the river continuum and interrupt the transport of organic matters and metals. In other words, they change the chemical and biological characterization of rivers ecosystems. This alteration in the configuration and flow regimen of the rivers also affects negatively to the river communities and riparian dwellers [8].

Thus, the main prospect for the future hydropower is to extract the kinetic energy form fluvial or marine currents through turbines without dams or any head water channel.

2.1.1.2 Water stream turbines

These turbines are located in the basin of river or in marine current. They are essentially similar to the traditional wind turbines, but they are placed under the water instead. The main difference when comparing these devices to wind turbines is that the rotors of stream turbines require smaller rotors if the same power is to be produced, since the density of the water is 800 times greater. These turbines can be classified into two groups, Axial Flow Water Turbines (AFWT) and Cross Flow Water Turbines (CFWT), Figure 3 [9].

- Axial Flow Water Turbines are machines whose axis of rotation is parallel to the direction of the water current.
- Cross Flow Water Turbine are machines whose axis of rotation is perpendicular to the direction of the water current.

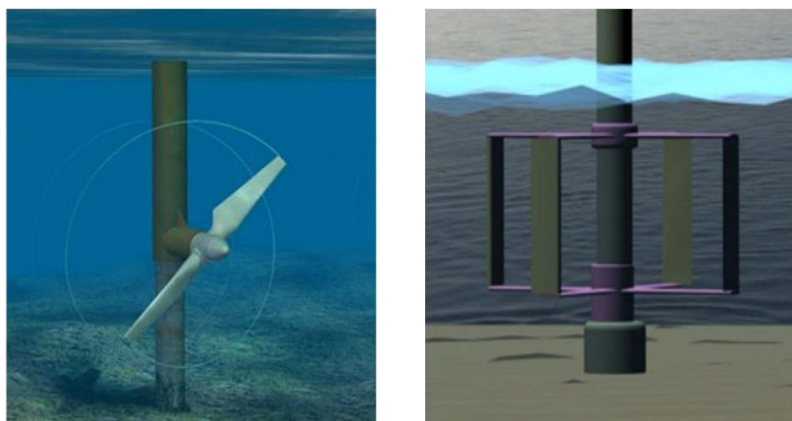


Figure 3. Water stream turbines, Axial Flow Water Turbine, and Cross Flow Water Turbine from left to right respectively [10].

2.1.1.3 Axial Flow Water Turbines

These machines consist in a propeller, normally with two or three blades fixed to a rotor. In these devices, the flow faces the plane of rotation perpendicularly, being the lift force responsible for the rotation of the turbines. The lift force is the force generated in an object placed in a stream which is perpendicular to the direction of the stream [10].

Therefore, the rotor of these devices must be controlled to follow the direction of the water flow. This movement is known as “yawing”. Without this orientation

system the efficiency drops drastically. Also, they need a pitch control in their blades to control the angular speed. However, they are not considerably influenced by the variation of the velocity of the flow. Thus, they achieve higher efficiencies in energy conversion when the flow changes frequently, as it occurs in wind turbines. Thereby reducing the expenses per kW in wind power [11].

2.1.1.4 Cross Flow Water Turbine

These types of devices could be either lift devices, drag devices (also known as “Panemons”) or a combination of both lift and drag. Figure 4 presents the three basic rotors, the two Darrieus and the Savonius turbines. While the Darrieus is mainly a lift-based turbine, the Savonius is a drag-based turbine. There are many different vertical turbines, however they can be considered modifications or combinations of the Darrieus and Savonius turbines [12].

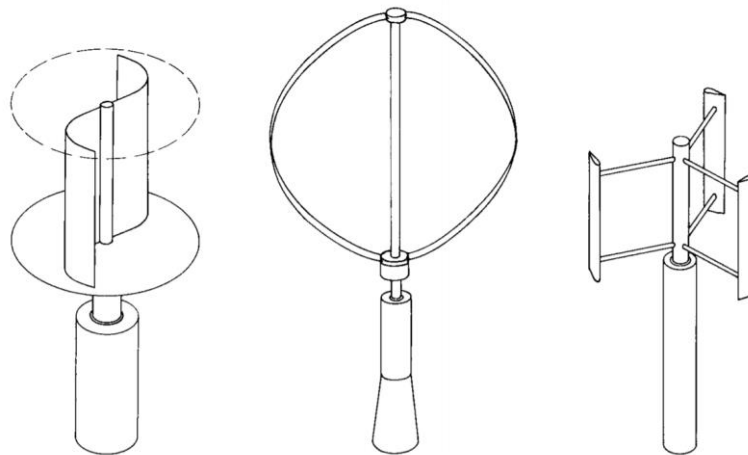


Figure 4. Vertical turbines, Savonius rotor, Darrieus rotor and H-Darrieus rotor respectively [12].

The major advantage of these turbines over the axial turbines is that they are independent of the flow direction. Hence, they do not need any mechanics of yawing to track the flow direction. The major disadvantage is the influence of the changes in the velocity of the flow. However, under constant flows, it was found that higher efficiencies can be achieved [12].

2.1.2 Turbines characterisation

As aforementioned water stream turbines extract the energy from the natural kinetic energy of a stream. This kinetic power can be calculated with equation (1). However, when the rotor swept area is not negligible compared to the cross-sectional area of the flow passage, the turbines can extract additional potential energy induced between upstream and downstream, thanks to the phenomenon known as blockage effect. This effect can be characterized by the coefficient given in equation (2), [13].

$$P_{kinetic\ available} = \frac{1}{2}\rho Au^3 \quad (1)$$

Where ρ [kg/m³] is the density of the flow, A [m²] is the projected area of the turbine perpendicular to the flow, and u [m/s] is the velocity of the flow.

$$B_L = (turbine's\ frontal\ area)/(Channel\ section\ area) \quad (2)$$

Nevertheless, turbines cannot extract all the kinetic energy from the flow. Even for the ideal turbine, it was proven that the maximum kinetic energy extracted is only $16/27 \approx 0.593$ of the kinetic energy available. This maximum is known as Betz limit [14]. Thus, a power coefficient is common used to characterize the rotors. This coefficient is known as C_p (equation(3)) and it is given by the ratio between the power output from the rotor and the energy of the water flow. However, this maximum in the C_p of $16/27$ is for the kinetic energy, hence when the blockage effect is not negligible, the C_p can take higher values as Garrett and Cummins (2007) proved. The Garret-Cummins model is essentially an extended version of the Betz theory and modifies the maximum C_p as equation (4) shows [13].

$$C_p = \frac{Power\ extracted}{Power\ available} = \frac{P_T}{\frac{1}{2}\rho Au^3} \quad (3)$$

$$C_{pmax} = \frac{16}{27} \cdot (1 - B_L)^{-2} \quad (4)$$

From equation (4) it can be concluded that the blockage effect has a significant importance in the performance of the turbine. When the blockage effect coefficient tends to one the C_p coefficient tends to infinity [13].

C_p can be considered the main parameter to assess the performance of turbines. This coefficient does not remain constant while the turbine is working. It varies as the Tip Speed Ratio (TSR or λ) changes and also depends on the angle of attack of the blades. The TSR is the relation between the speed of the blades and the flow speed. It can be defined as follows [15]:

$$TSR = \frac{\text{rotor blade tip speed}}{\text{Water speed}} = \frac{R \cdot \omega}{u} \quad (5)$$

Hence it is possible to obtain the C_p of the turbine as function of the TSR. Since the velocity of the flow it is not constant, the angular velocity can be modified by modifying the load on the generator. This way the turbine can be working in its optimal point always. Figure 5 shows the C_p of different turbines as function of the TSR [15].

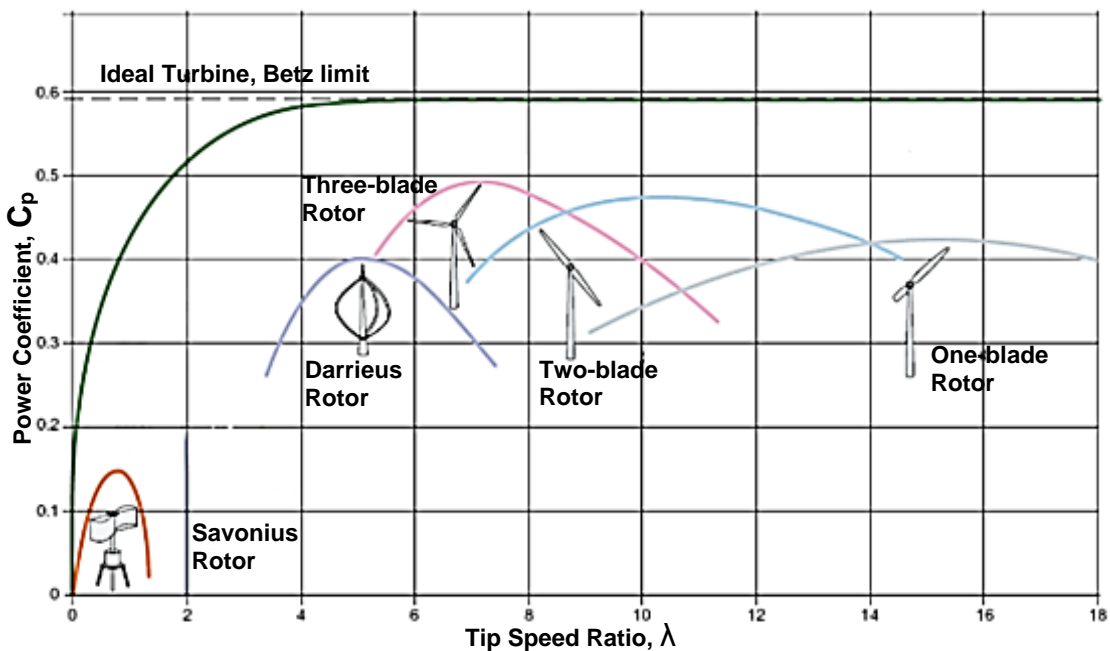


Figure 5. Power coefficients of rotors with different TSR [15].

2.1.3 Drag-Based turbines

The drag-based turbines are devices that generate a torque around their axis due to asymmetric drag force that the flow induce on their blades. The drag force can be defined as shown in equation (6) shows.

$$F_D = \frac{1}{2} \cdot C_D \cdot \rho \cdot A \cdot u^2 \quad (6)$$

where C_D is the drag coefficient, that depends on the shape of the bodies.

Typically, asymmetric drag is due to the shape of the blades, since different geometries will result on different drag coefficients. If Savonius turbine is taken as an example, it is easy to see how the static torque is generated on Figure 6 [16].

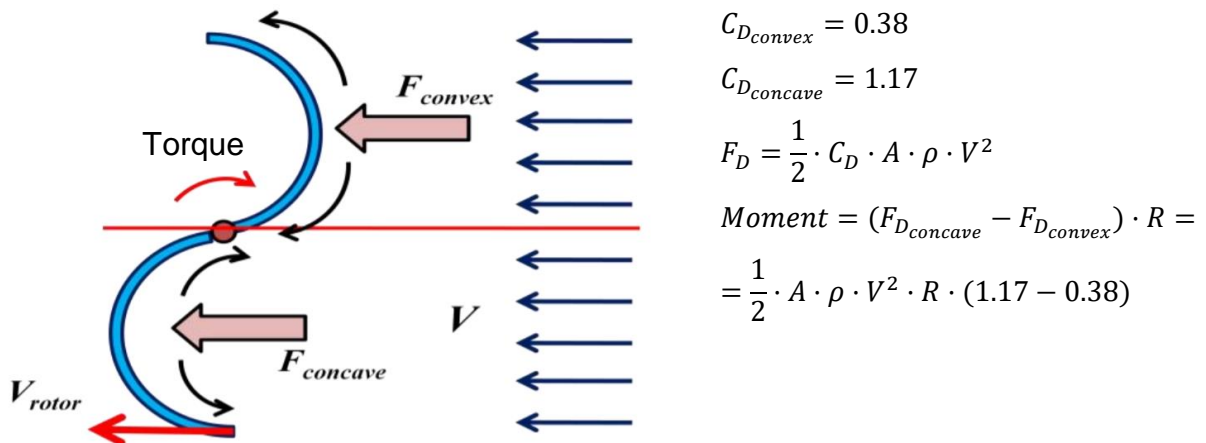


Figure 6. Schematic drawing showing the drag forces exert on two blade Savonius [16].

When the turbine is not static, and it is rotating the velocity of the flow on the blades is not the same as the result of the relative velocity of the blades with respect to the flow. The convex blades will have higher velocity, therefore the drag force will be bigger. Conversely, in the concave blade the velocity is lower, consequently the drag force is lower. This will result on a lower torque. Thus as the rotor goes faster, lower it is the torque [16].

From the previous explanation it possible to figure out the main advantage of these kind of turbines:

- High starting and operating torque.
- The tip speed ratio is low, the turbine rotates at lower speed than the air which makes the rotors more durable.
- Mechanism to avoid the rotor to runaway is not necessary since the turbine always rotate at low velocity.
- The simplicity of these turbines makes the devices cheap and with low maintenance.

In this project a turbine with the same principle explained previously is developed. However, the main difference is that the blade which does not contribute to the torque does a pitch motion in order to minimize the drag by reducing the area that the flow faces [17].

2.2 Computational Fluid Dynamics

Computational fluid dynamics CFD is the current state-of-art technique in fluid flow analysis. It has been proven to be one of the most cost-effective tool and widely used for simulation, analysis and design turbines with complex flows [2].

The application of CFD is extremely wide, however the most common applications are Aerodynamics for vehicles and aircrafts, turbo-machinery, power plants, marine engineering, process industries, biomedical engineering etc. Besides, it considered to be a powerful alternative design tool which provides an insight into flow characteristic in hydropower components. Many investigations have studied the performance of turbine (i.e. prediction of the load, cavitation of the rotor, iteration between the rotor and the stator...) through numerical simulations in CFD [18].

Nevertheless, to the best of my knowledge, a few number of CFD works have been performed on drag-based vertical axis turbines. It was highlighted in other studies [19] CFD simulations to analyse the performance of rotors can be performed in a cost effective manner, as compared to scaled tunnel experiments and field tests. One of the first simulations of CFD on vertical axis turbine was performed in 1995 by Fujisawa et al. in which they predicted the pressure contours from steady simulations in a two-dimensional RANS model.

Then Kawamura et al. simulated a Savonius configuration using a domain decompositions RANS approach to characterise the dynamic torque [20].

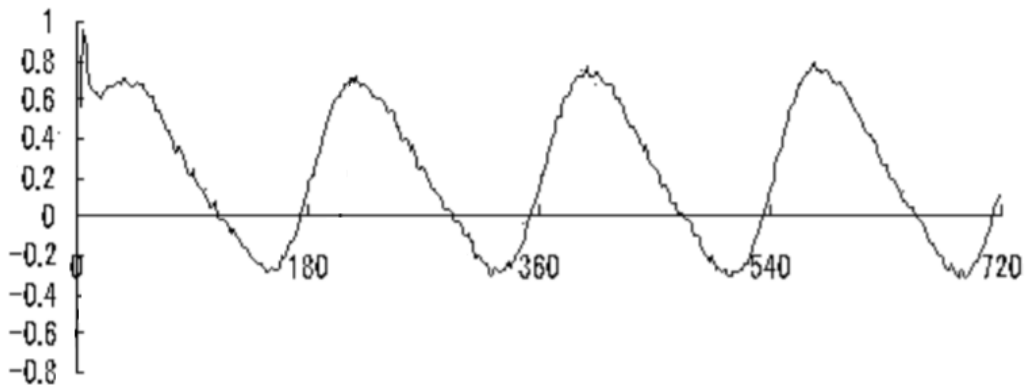


Figure 7. Kawamura simulation, time history of the torque coefficient vs the angle of rotation (Tip speed ratio is 0.25) [21].

More recent studies, such as the one carried out by Mohamed et al. used RANS and evolutionary algorithms to investigate the effect of obstacles upstream to reduce the negative torque contribution [20].

Other researchers have done similar works to the present one, designing alternatives to Savonius rotors. For example, the Aeolun Harvester[®], designed by T. Sankar is an alternative design which was assessed by means of CFD. They aimed to design an inexpensive and simple turbine [22].

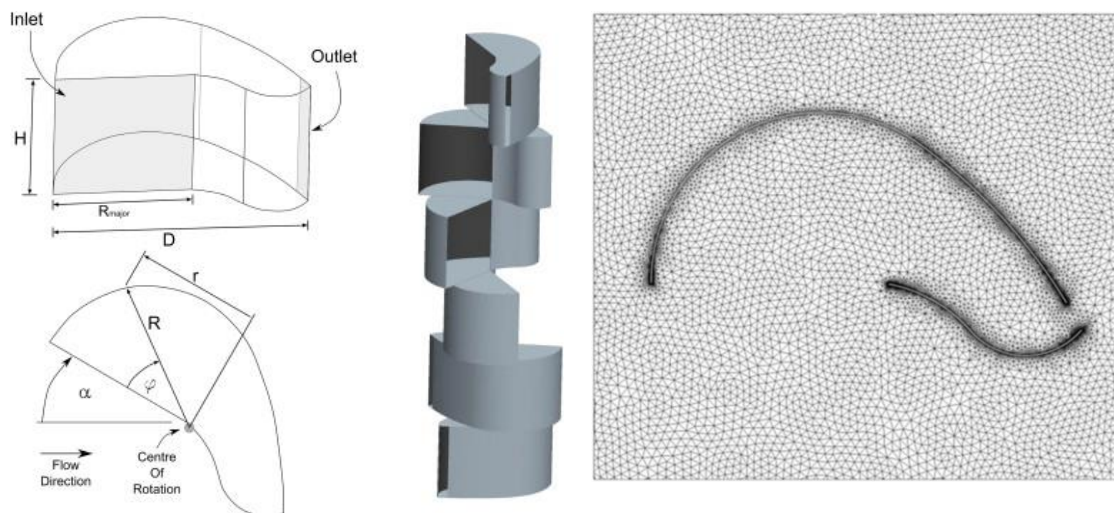


Figure 8. Wireframe view and solid model of the Aeolun Harvester design and its mesh for the simulations [20].

3 Proposed concept

Once the background of vertical turbines has been described, especially of drag based turbines, it is time to proceed with the explanation of the design of the proposed concept which made place to this work.

The concept is really simple, it is based on straight blades connected by a shaft Figure 9. The turbine has two degrees of freedom. Firstly, the “y” axis which is the axis that the turbine rotates around. (in this case clockwise direction has been selected). Secondly, a rotational degree of freedom around “z” axis. Note that this rotation is constrained to 90 degrees. The constraint is shown in the Figure 9 as “ β ”, which can take any value between 0° and 90° .

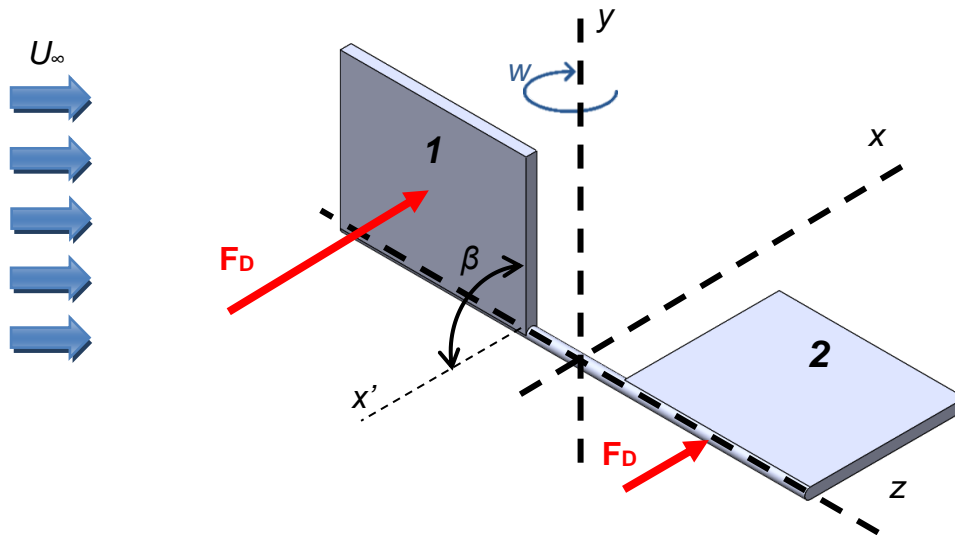


Figure 9. Diagram of velocities and drag forces of the turbine.

Thus, when the fluid goes through the turbine, it will face the blade number one perpendicular and the number two parallel to the flow. In this case, the drag force (equation (6)) will be much bigger in blade one than in blade two due to the area that the flow faces. This generates a torque around “y” axis in the direction of the rotation because “ β ” cannot take a higher value than 90 degrees. Then as the turbine rotates, the shaft will be aligned with the “x” axis and the fluid will start to generate the drag force in the other surface of the blade one. This force on the other face of the blade one will generate a torque around the shaft. This movement now is possible (“ β ” can take lower values

Proposed concept

than 90°) and this pitch will finish when the blade one is parallel to the plane XZ ($\beta=0^\circ$). Once the pitch is done the blade two starts to generate torque and the blade one is parallel to the fluid in order to produce as lower drag as possible. This sequence is represented in the Figure 10. In Figure 10 (c) the pitch can be seen.

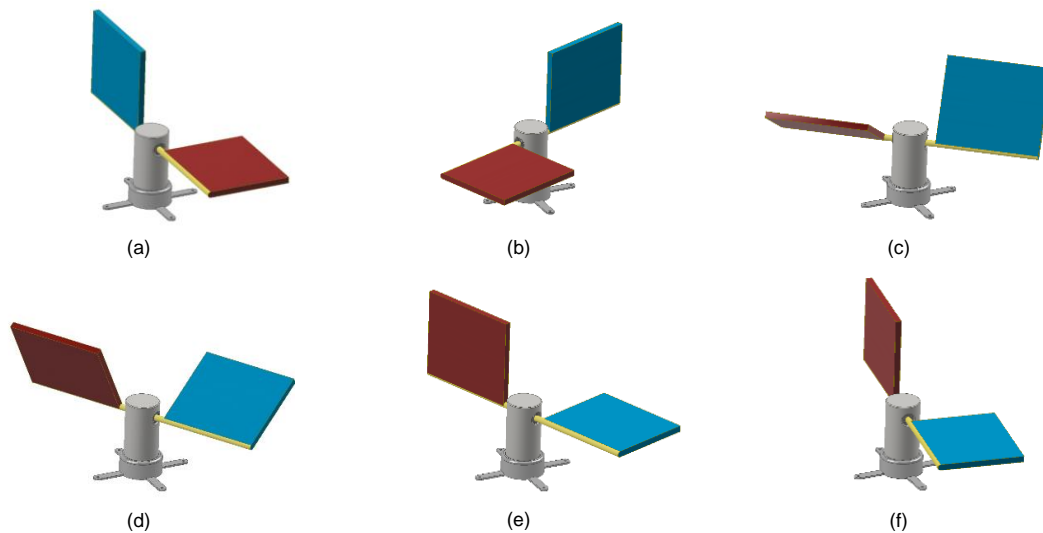


Figure 10. Sequence of half lap of the turbine represented with the flow from right to left.

In the previous sequence it can be seen already blades with the main shaft and the support which will be grounded on the bed of the water channel. In the following figure it is possible to see a realistic picture where the arrangement of the turbine in the channel is shown.

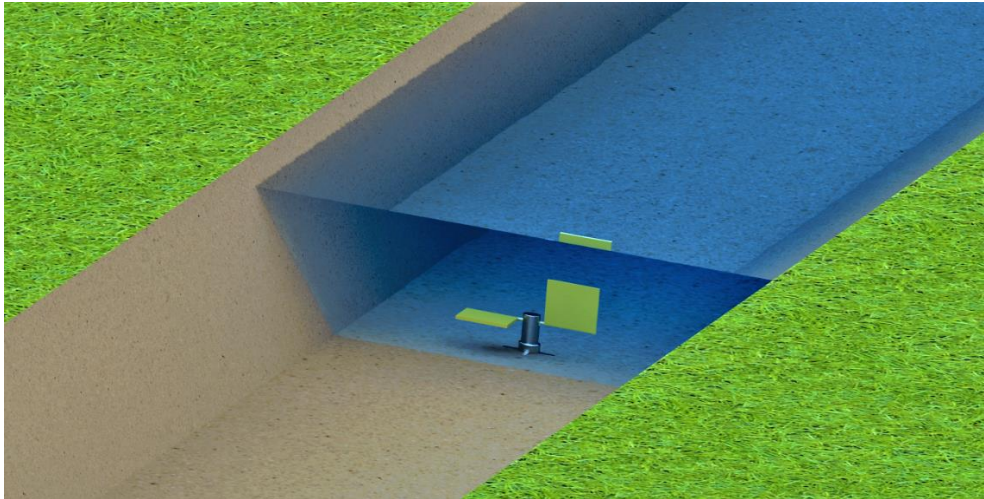


Figure 11. Render of a possible position of the turbine in a channel.

Since it is grounded on the bottom of the channel one thing to take into account is that the velocity of the flow next to the bottom is zero. This is possible to see in Figure 12 where the velocity profile of a river can be seen.

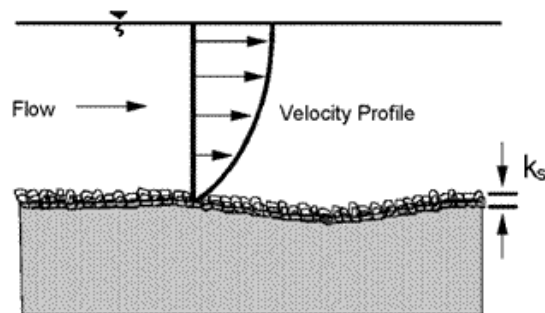


Figure 12. Velocity profile of a random channel of water [23].

Taken this into consideration, the geometry of the turbine can be adapted in order to avoid the placement of the turbine to low in the bottom of the water channel. However, this fact will be discussed later on.

To conclude this section the prototype design in SOLIDWORKS is presented Figure 13. It is possible to see that inside the main shaft there are place two blocks. Thus, due to the piece that the shaft has in its middle (blade block), the rotation of the blades is limited between the other two blocks i.e. 90 degrees.

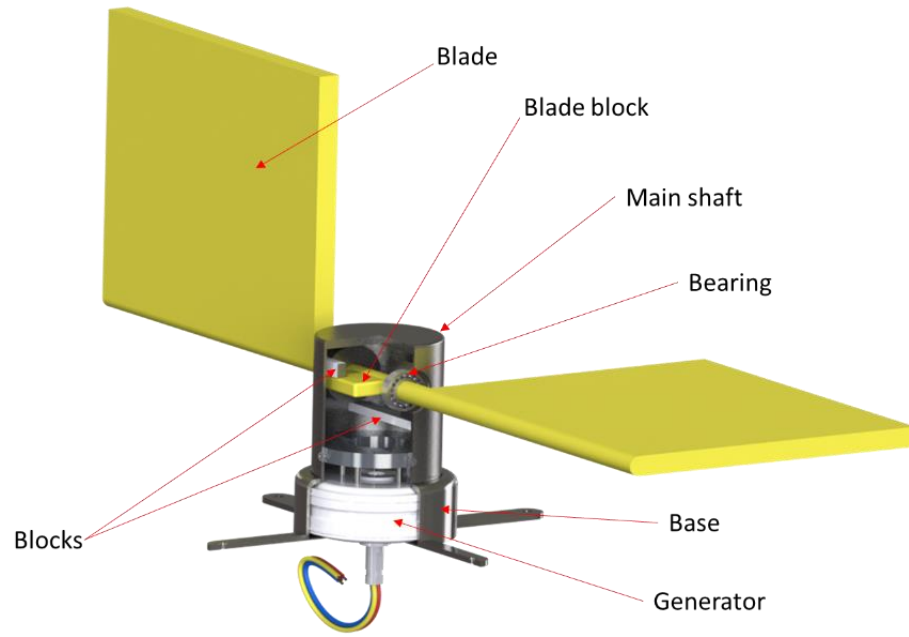


Figure 13. Render of the prototype proposed with the name of each part.

4 Methods

In this section, the methodology used in this work is presented. The aim of this method is to determine the operating parameter of the novel turbine. First the geometry of the turbine is explained, and then the CFD model.

4.1 CFD model

Given the concept of the turbine explained on the section 3 the first step is to create the geometry, a domain to work with.

4.1.1 Geometry

The domain of the model was created with SOLIDWORKS 2017 software and exported as a STL file. The designed geometry was a simple channel, of rectangular section with an inner domain of cylindrical shape. Then, inside the inner domain the blades of the turbine were subtracted to the body. The result was two bodies the outer domain that contains a cavity for the inner domain and the inner domain that contains a cavity with the shape of the blades as it is described in Figure 14.

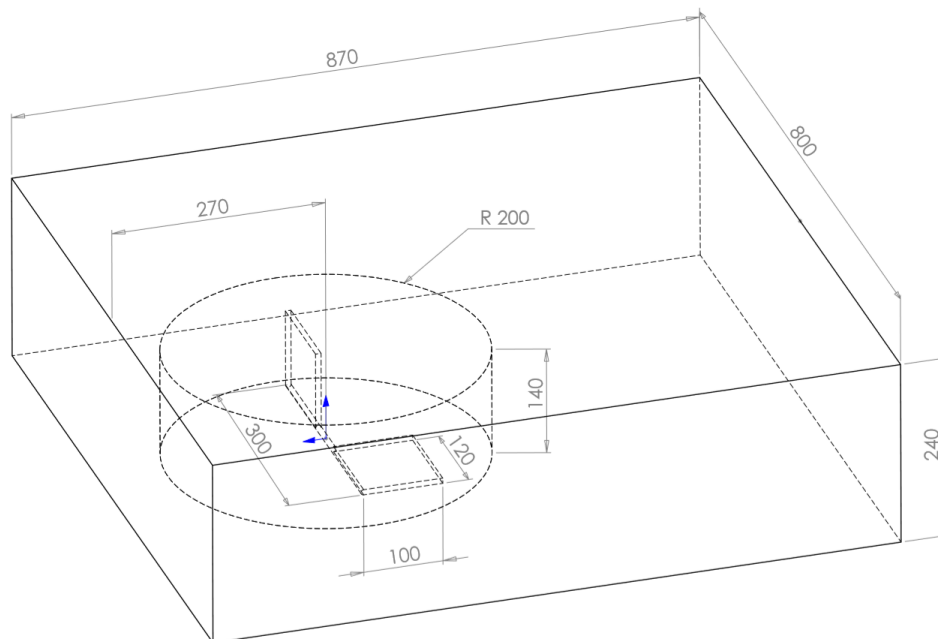


Figure 14. Wireframe view of the entire domain. The dimensions are in mm.

Methods

The blades are composed of two plates, 103.5 mm high and 120 mm wide. They are connected by a 300 mm length and 7 mm diameter shaft. Therefore, the gap between the blades is 60 mm. However, the dimensions of the blades have been modified as required for different simulations to analyse the influence of their geometry on the performance of the turbine. Yet, these dimensions were taken as reference for other simulations.

Furthermore, in order to facilitate the post-processing of data a control volume was created in front of the turbine (Figure 15). The aim of this volume is to provide a reference where the flow of the water that passes through, can be calculated. This flow is assumed to be the same as the flow through the turbine. This flow is an important parameter since the C_p , (equation (3)) is calculated based on the velocity of the flow through the projected area of the turbine. Hence, the resultant geometry of the model is composed of three different bodies: the outer domain, the inner domain and the control volume.

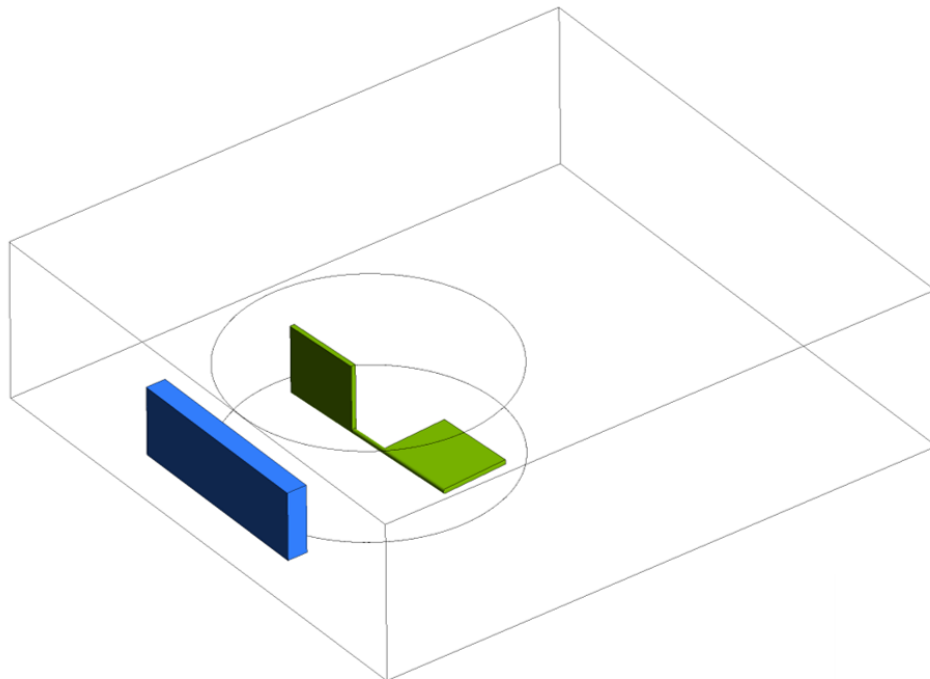


Figure 15. Wireframe view of the entire domain showing the control volume used to calculate the velocity of the flow.

4.1.2 Mesh

The following step after defining the shape of the domain was to import the STL file in the Workbench 18.2 of Ansys® and to mesh the geometry. The meshing of the domain can be accomplished by different means. However, the most common method adopted in 3D CFD models is based on tetrahedral or hexahedral volumes. The mesh based on tetrahedral is known as unstructured mesh while the structured meshes are those based in hexahedrons. In this particular configuration the mesh of the inner domain has to be unstructured since the model uses dynamic mesh¹ in that zone [24].

Even if the structured mesh can provide higher accuracy in some cases, the unstructured mesh is preferable when solving complex geometries due to its flexibility [18]. Thus, tetrahedrons have been used for the whole model. In addition, inflation layer was considered around the blades. However, the problem with the inflation layer was that the mesh around the blades adapted and remeshed every time step due to the pitch motion of the blades. During this movement, if during one time step the blades move more than the size of one element the simulation crashed. Therefore, if the elements around the blades are too small the time step must be small also. In short, the inflation layer generates tiny elements around the body. In the simulation running during this study they would crash even during working with time step lower than 0.1 μ s. This is unacceptable considering that turbine simulations should last around 7 laps to achieve the steady state [25] which corresponds with simulation between 72 and 14 seconds in the cases studied.

Consequently, the domain was meshed with tetrahedrons, the different meshes used cover from 276088 to 1730561 elements. Furthermore, taking advantage

¹ **Dynamic mesh:** The dynamic mesh is used for moving and deforming bodies where the mesh must adapt to the movement. It has showed good result for problems with oscillations of small amplitude or deformation however for big displacements this method may lack its robustness and it needs to be used together with grid remeshing methods [31].

of the meshing tool of Ansys® the different parts of the domain were named. In the Figure 16 the meshed domain and the names of the different parts are shown.

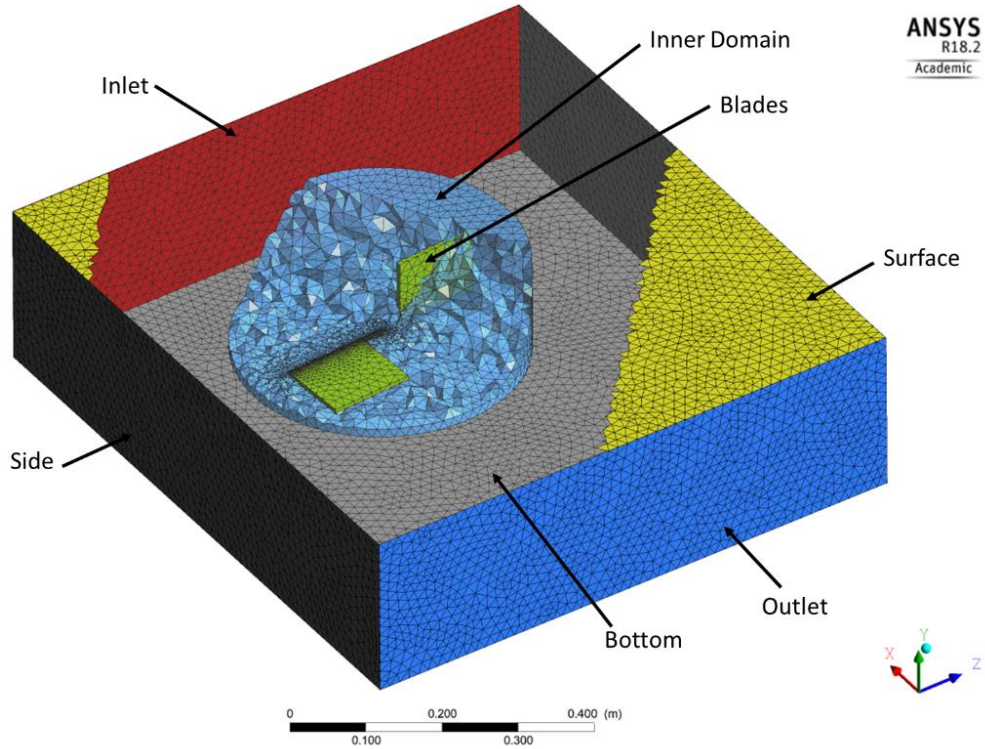


Figure 16. Domain, mesh and named parts of the geometry.

In this figure, the mesh in the outer domain was removed in order to show details inside. Besides, the inner domain was cut to show the blades inside and the top limit of the domain was cropped as well. The boundary conditions will be detailed in the following section. However, taking advantage of the previous figure it is possible to anticipate the boundaries. In the grey region the sides and the bottom of the channel which are defined as walls. Then the inlet and outlet are in red and blue respectively and in yellow the surface which is defined as symmetry [26]. The surface of the inner domain is defined as contact region and finally, the cavity inside the inner domain in green, which correspond to the blades, are defined as walls.

4.1.3 Set up of the simulation

The simulation performed is required to be as close to the real conditions as possible, in order to do that the CFD technique used was the finite volume calculation and the software used was Ansys® Fluent v. 18.2.

The objective of the simulation was to calculate the power generated by the turbine. In order to do that, unsteady incompressible Reynolds Average Navier Stokes (RANS) simulation was performed.

The behaviour of the fluid during the simulation is based on the continuity equation (the inflow matches the outflow) and the momentum conservation of Navier-Stokes which are given by equation (7) and (8) respectively. In addition, the fluid, was considered incompressible and the temperature variation was neglected.

$$\frac{\partial \rho}{\partial t} + \nabla \cdot (\rho \vec{u}) = 0 \quad (7)$$

$$\frac{\partial \rho \vec{u}}{\partial t} + \nabla \cdot (\rho \vec{u} \vec{u}) = -\nabla P + \nabla \bar{\tau} + \rho \vec{g} + \vec{F} \quad (8)$$

where ρ is the density of the flow; t is the time; u is the velocity vector; $\rho \vec{g}$ is the gravitational body force; \vec{F} is the external force; and $\bar{\tau}$ is the stress tensor.

For the simulation, the two equation κ - ε model for eddy viscosity known as Re-Normalization Group (RNG) turbulent model was used. The model is based on the transport of turbulent kinetic energy contained within the fluctuations “ κ ” equation (7) and the turbulent energy dissipation rate “ ε ” equation (8).

However, it should be mentioned that the equations κ - ε used are not considered to be conservation laws, like the equations explained previously. In fact, the eddy viscosity is employed, which is a parameter based on guesswork [27].

$$\frac{\partial(\rho k)}{\partial t} + \frac{\partial(\rho k u_j)}{\partial x_j} = \frac{\partial}{\partial x_j} \left[\frac{\mu_t}{\sigma_k} \frac{\partial k}{\partial x_j} \right] + 2\mu_t E_{ij} E_{ij} - \rho \varepsilon \quad (9)$$

$$\frac{\partial(\rho \varepsilon)}{\partial t} + \frac{\partial(\rho \varepsilon u_j)}{\partial x_j} = \frac{\partial}{\partial x_j} \left[\frac{\mu_t}{\sigma_\varepsilon} \frac{\partial \varepsilon}{\partial x_j} \right] + C_{1\varepsilon} \frac{\varepsilon}{k} 2\mu_t E_{ij} E_{ij} - \rho C_2 \frac{\varepsilon^2}{k} \quad (10)$$

where E_{ej} is the rate of deformation; μ_t is the eddy viscosity; σ_k and σ_ϵ are the Prandtl numbers for k and ϵ ; and $C_{1\epsilon}$ and $C_{2\epsilon}$ are the constants which fit the selected data.

Other aspect to consider was the surface of the domain which is in contact with the air. The iteration between the free surface of the water and the air can be simulated using Eulerian Volume of Fluid (VOF) which requires the multiphase model [28]. However, this approach was not feasible due to the complexity of the current model. Otherwise the computational effort would be unaffordable.

Additionally, it has been proven that when the analysis of the free surface of the water is not the main objective of the study, the boundary condition of the surface can be modelled as symmetry. This boundary sets the normal velocity of the surface and the normal gradients of all variables equal to zero [26].

Firstly, before explaining the boundary conditions of the model, the approach followed to simulate the turbine needs to be described. As it was explained in the section 2.1.2 Turbines characterisation the main parameter that defines the performance of a turbine is the C_p which depends on the tip speed ratio (λ or TSR) and the geometry of the blades. Hence simulations with different TSR are needed in order to characterise the turbine. However, this will be further explained later on. Bearing this in mind, simulations where the turbine rotates at constant velocities have been carried out. For each velocity, the C_p of the turbine was calculated. This way, the characteristic curve of the turbine can be calculated as in Figure 5.

Besides the rotation of the turbine, the pitch of the blades needs to be set which was explained in section 3. This pitch is simulated using dynamic mesh as it was briefly mentioned above. In order to do this, three different approaches were considered:

- Inner domain rotating and deforming, i.e. inner domain with mesh motion as well as dynamic mesh, Figure 17 b.
- Inner domain rotating and deforming, i.e. inner domain with dynamic mesh as well as dynamic mesh motion, Figure 17 b.

- Inner domain deforming and the outer domain rotating, i.e. inner domain with dynamic mesh as well as outer domain with mesh motion, Figure 17 c.

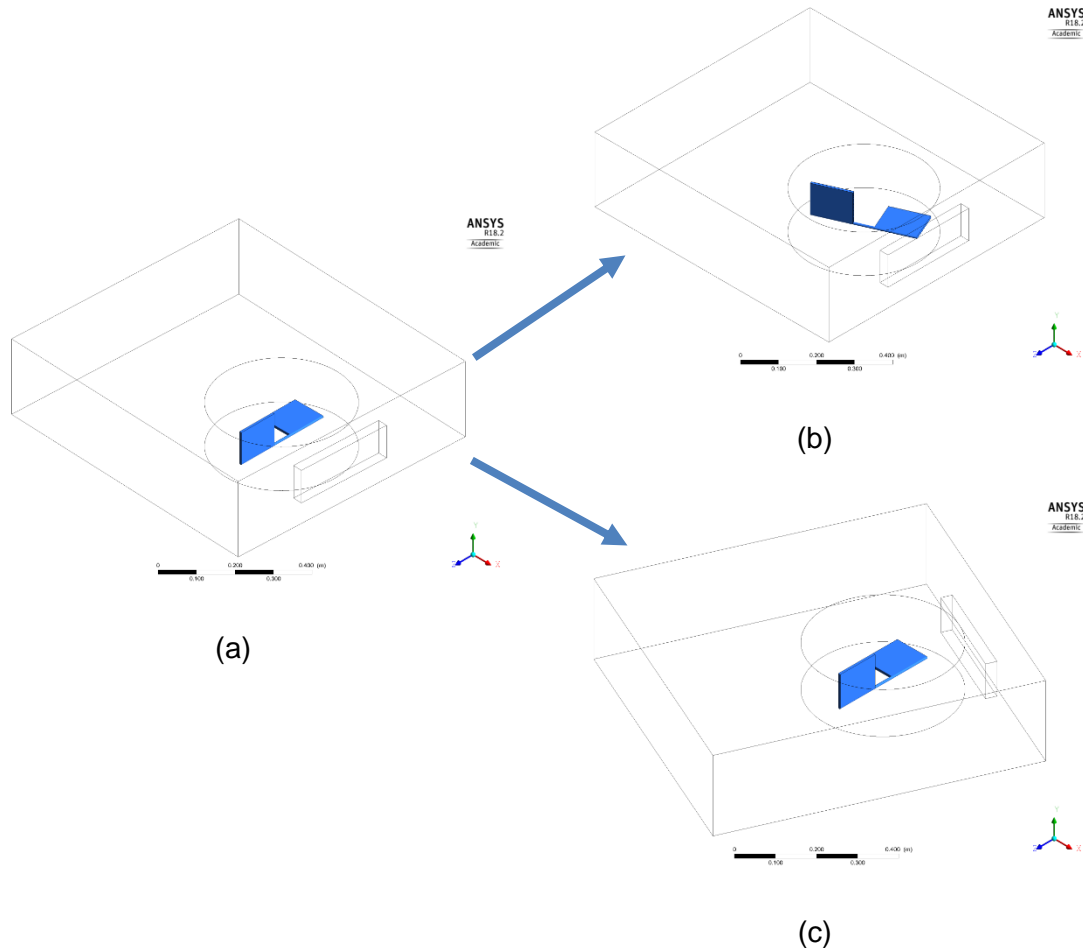


Figure 17. Different approaches for the model, (a) beginning of the simulation $t=0$ s, (b) $t=2$ s inner mesh moving, (c) $t=2$ s outer domain moving.

The simplest case is the first one where the inner domain is defined with dynamic mesh and mesh motion. The dynamic mesh in this case was defined as one degree of freedom (DOF) rotation around the local “z” axis of the blade. This axis also corresponds the axis of the shaft. On the other hand, the mesh motion was defined with a constant velocity around the global “y” axis.

Nevertheless, this configuration did not work. In fact, the mesh motion defined on the “cell zone” and the dynamic mesh do not interact with each other; thus it cannot be used to couple the movements. This configuration resulted in the turbine rotating randomly around its centre. The turbine rotated around the “y”

Methods

axis but the degree of freedom was set as a rotation around the global “z” axis instead of the local “z” axis (which is rotating with the blade). Despite it might look like something easy to solve, this approach is not feasible as the Ansys® support stated.

The second approach is similar to the first one but instead of mesh motion it used dynamic mesh motion. The dynamic mesh motion is a macro of the dynamic mesh and it should be coded as an User defined function (UDF). This macro allows the user to set the dynamic mesh and a force, but not a velocity. In many cases, it is easy to convert a force into a constant velocity. Yet for vertical axis turbine, it is not that simple as the torque that governs the turbine is not constant.

Consequently, the approach taken was the third one. It might look less intuitive and more complex a priori, but it is the most realistic for this work. In this configuration the flow perceived by the turbine is the real one, it is just a matter of relative velocities. The idea is that the outer domain (the fluid around the turbine) is set as moving mesh with constant speed. Therefore, the inlet, outlet and all the boundary conditions of the outer domain are rotating solidary, so the flow goes straight from the inlet to the outlet independent of the rotation of the domain. Then, inside this rotating domain the inner domain is placed which is not rotating. Thus, the deforming dynamic mesh can be set without the problems of reference above mentioned.

The next step was to set the dynamic mesh, one degree of freedom rotation around “z” axis was defined. This corresponds to the shaft axis along the whole simulation since the inner domain remains static. This degree of freedom was constrained 90 degrees (to constrain the pitch) and the inertia around the “z” axis was set. The inertia was a problematic parameter as it will be explained ahead in this report.

The following step was to set up the boundary conditions (Figure 16) of the model, where the blades, the bottom and the sides were defined as normal walls. The inlet was defined as velocity inlet and fixed in 1 m/s for all the simulations. It should be defined as normal to the surface of the inlet, however

Methods

Fluent stops working when it is set. The solution to this problem was to set the velocity direction through cylindrical components. In addition, it is possible to set an angular velocity to this cylindrical component, which was set with the same value of the angular velocity of the outer domain. The turbulent intensity was set to 5% and the turbulent viscosity ratio to 10.

The outlet was defined as pressure outlet, in this case, it was possible to set the pressure outlet normal to the surface and with a gauge pressure of zero. This means that there is a difference of zero Pascals with the reference pressure, which was set in the point (-0.6, 0.2, 0) to atmospheric pressure. The previous point corresponds with the middle point of the intersection of the inlet with the surface. Besides, the outlet was set to 5% of turbulent intensity and to a turbulent viscosity ratio of 10 as well.

The surface was defined as symmetry, as discussed previously. This means that the normal velocity of the surface and the normal gradients of all variables are equal to zero in this area.

Finally, different data files were created, with data every time step. One of these data files to collect the values of the caudal through the control volume that was created. As aforementioned, this flow is assumed to be flow through the swept area of the turbine. Then, another file was created with the position of the blade, in order to know the angle “ β ” of the pitch Figure 9. Finally, one more file with the moment coefficient (C_m) around the “y” axis was created, in order to calculate the torque generated by the blades. The C_m can be defined as follows [29]:

$$C_m = \frac{\text{Torque}}{\frac{1}{2}\rho U^3 A_{\text{sweep}}} \quad (11)$$

The previous formula can be combined with the equation of the C_p equation (3) to obtain the following equation [30]:

$$C_p = C_m \cdot \lambda \quad (12)$$

4.2 Analytical solution

One of the main requirements for every CFD model its validation. The most reliable method, and sometimes the only method, to validate the model is through experimental data. However sometimes experimental data is not available as happened in this study. Owing to the simplicity of the model studied it was possible to develop an analytical model through basic equations. Following the explanation on sections 2.1.2 and 2.1.3 the analytical model is explained bellow. The drag force for each part of the blade i.e. for each plate was calculated. Thus, the velocity on equation (6) is defined as:

$$V_1 = U_\infty - w \cdot R \cdot \cos(w \cdot t) \quad (13)$$

$$V_2 = U_\infty - w \cdot R \cdot \cos(w \cdot t - \pi) \quad (14)$$

where w is the angular velocity of the turbine; t is the current tie; and U_∞ is the velocity of the flow.

The equations (13) and (14) are based on the Figure 18. These equations provide the velocity of the flow perceived by the centre of the blade.

Then in equation (6) they can be substitute the above equation and the drag forces and the torque are defined in equations (15), (16) and (17) respectively. If equation (13) and (14) are introduced in equation (6), the drag forces and torque can be defined as follow, equations (15), (16) and (17).

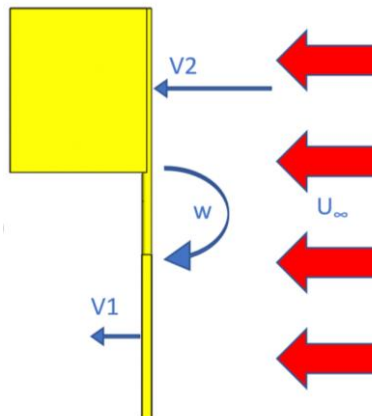


Figure 18. Velocities diagram of the blades.

$$F_{D1} = \left(\frac{1}{2} \cdot C_{D_{blade}} \cdot A_{blade} \cdot \rho \cdot V_1 \cdot |V_1| - \frac{1}{2} \cdot C_{D_{shaft}} \cdot A_{shaft} \cdot \rho \cdot V_2 \cdot |V_2| \right) \cdot \sin(\beta) \cdot \cos(\omega \cdot t) \quad (15)$$

$$F_{D2} = \left(\frac{1}{2} \cdot C_{D_{blade}} \cdot A_{blade} \cdot \rho \cdot V_2 \cdot |V_2| - \frac{1}{2} \cdot C_{D_{shaft}} \cdot A_{shaft} \cdot \rho \cdot V_1 \cdot |V_1| \right) \cdot \cos(\beta) \cdot \cos(\omega \cdot t + \pi) \quad (16)$$

$$Torque = (F_{D1} + F_{D2}) \cdot R \quad (17)$$

The second term of the equations above corresponds to the drag generated by the plate which is not perpendicular to the flow. In addition, the equations are multiplied by sine and cosine factor. Hence when the blade one is perpendicular to the flow ($\beta=90^\circ$) the drag force F_{D2} is zero and the other way around. Only during the pitch, both drag forces (F_{D1} and F_{D2}) take values different to zero simultaneously.

Despite the equations above being drag force equations they differ from equation (6) in the velocity term. According to equation (6) the velocity should be raised to the power of two, however in this case is $V_1 \cdot |V_1|$ in order to preserve the sign of the velocity.

Once the forces are calculated the torque is easily extracted from equation (17) and the power can be calculated with the equation bellow equation (18). Finally, the C_p can be calculated with the equation (3).

$$P = Torque \cdot \omega \quad (18)$$

Up to this point, the model is able to calculate the C_p using the data of the motion of the pitch as an input. This data is provided by fluent. Thus, one approach of the analytical validation consists on taking this value from Fluent and comparing the C_p calculated by the analytical model proposed and Fluent.

However, the angle β can be calculate analytically too. This second approach is also based on the equations of the drag (15) and (16). The motion of the pitch is calculated when either F_{D1} or F_{D2} have a negative value. In fact, these forces

are the ones responsible for the initiation of the pitch motion. Figure 19 shows the forces generated in the blade when the drag force is negative.

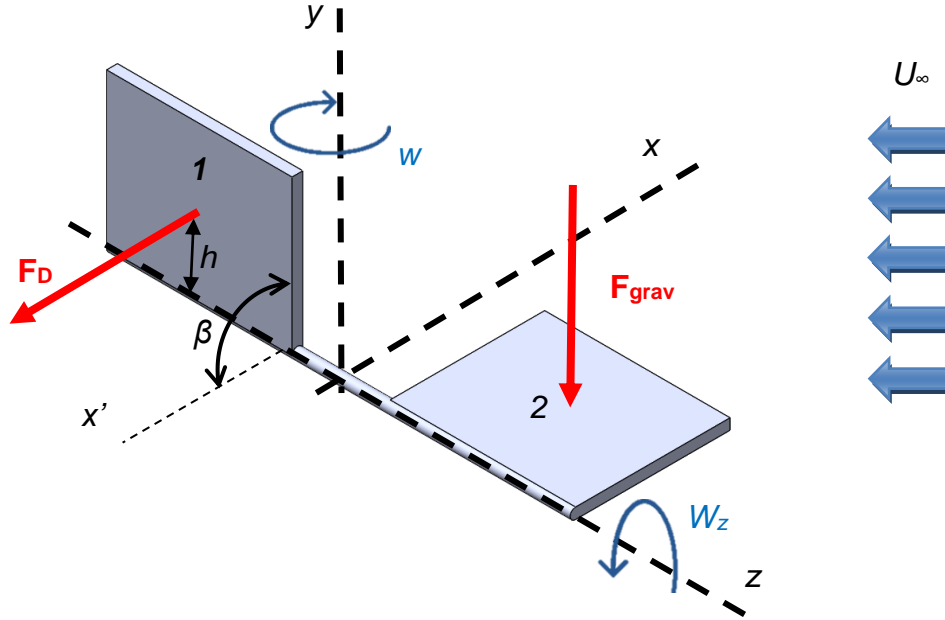


Figure 19. Diagram of the pitch force and velocities. Where the forces are in red and velocities in blue.

The drag force will generate a torque around the “z” axis. As it was explained previously the rotation in this axis is not totally constrained, 100% it can rotate 90 degrees, from $\beta=90$ (the current position of the figure) to $\beta=0$. When this drag force is greater than the gravity force, it induces an acceleration around “z” This acceleration can be calculated as follows.

$$\alpha_z = \frac{Torque_z}{I_z} = \frac{(F_D - F_{grav} - F_{added\ mass}) \cdot h}{I_z} \quad (19)$$

where α_z is the angular acceleration around z axis; h is the distance from z axis to the centre of the blade; $F_{added\ mass}$ is the force due to the added mass²; and I_z is the inertia of the blades around z axis.

² **Added mass:** is a term proposed by F. Besset in 1820, when he realised that the period of oscillation of a pendulum in a fluid is higher than in vacuum. “It is like the pendulum has a higher mass, or better moves a certain volume of water with it”. Actually, the fact is that due to the acceleration of a body the surrounding fluid accelerate as well. Thus, a force acting on a body has to accelerate the body and a portion of the fluid surrounding. It can be viewed as if the body has an added mass [32].

This acceleration generates a velocity and this velocity around “z” axis. Which modifies the angle β . The equations of motion which govern this phenomenon are:

$$w_z = w_{z_0} + \alpha_z \cdot t \quad (20)$$

$$\beta = \beta_0 + w_z \cdot t \pm \frac{1}{2} \alpha_z \cdot t^2 \quad (21)$$

Once β is calculated the analytical model is finished. The model was built in MATLAB and is attached in the Appendix A, where the codes developed can be found.

4.3 Sensitive analysis and validation

The validation of this work was based on the developed analytical model. All the results were compared with the analytical solution in order to validate them.

For the sensitive analysis at least three simulations are required. The coarse, the optimal and the fine mesh. The fine mesh has a huge number of elements and the result should not differ much from the optimal (usually less than 5%). The coarse has little elements but the result is significantly different from the optimal and the fine mesh. Finally, the optimal has the right number of elements, balancing the computational effort and the accuracy of the model (minimization of the error as compared to the fine mesh). Four simulations in which the number of elements were varied were performed.

4.4 Finding the optimal Tip Speed Ratio

As aforementioned, the C_p is the main parameter used to assess the performance of turbines since this coefficient gives the fraction of energy that the device extracts from the flow. This parameter is a function of the geometry of the blades and the tip speed ratio (TRS). Hence one of the first objectives was to find the characteristic curve of the turbine. In order to do that different simulations with different velocities were performed.

The idea was to modify the angular velocity of the outer domain and of the inlet reference, keeping the rest of parameters constant. The angular velocities

chosen were 0.3, 0.7, 1 and 1.3 rad/s; which correspond to a TSR of 0.024, 0.056, 0.08 and 0.1, respectively.

4.5 Influence of the inertia around the shaft

The inertia around the shaft was considered to be an important parameter beforehand. The higher the inertia, the more the time it needs to do the pitch. Also, it will increase the negative drag force leading to less torque and less power generation.

The inertia of the blades around the shaft was calculated with SOLIDWORKS software. The blades were set with a constant and reasonable thickness (7 mm) and the material used to model the turbine was aluminium. The inertia of this geometry is $0.00015 \text{ kg}\cdot\text{m}^2$. However, when the simulation was set with this inertia the blades started to oscillate. These oscillations every time step until the simulation crashed some time steps later. The oscillations before crashing could be the order of 10^0 in 0.0008 seconds, which are quite abrupt oscillations.

The inertia was increased to $0.0005 \text{ kg}\cdot\text{m}^2$ which is about three times the theoretical inertia. This inertia was taken as reference for all the simulations, However, how this parameter affects the performance of the turbine was studied as well.

In order to evaluate its influence, three different simulations with three different inertias were studied. All the other parameter remained constant and the inertia took values of 0.0003 , 0.0005 and $0.0007 \text{ kg}\cdot\text{m}^2$.

4.6 New configurations

After finding the optimal TSR some modifications are proposed to improve the C_p . Firstly, the geometry and the arrangement of the blades can be optimised. Therefore, the width, the height and the radius of the turbine can be modified. However, this has been left out of the scope of the project, as there are too many parameters to take into account. So, if a proper study is to be carried out many simulations should be run. This results in high computational effort which is the main limiting parameter of the work.

Methods

Hence the geometry was optimized with MATLAB software, based on the analytical model aforementioned.

The turbine was also modified by adding blades. First one pair more of blades were added and then one simulation with 4 pair of blades was performed. These simulations were set it with the reference values of 1 rad/s and 0.0005 kg·m² of inertia.

Finally, twisting the blades was considered, in order to increases the area of the blade while the turbine rotates towards the perpendicular position. This would generate more drag which leads to increasing the C_p . However, one of the main advantages of this turbine is the simplicity. This twist of the blade will complicate the geometry of the turbine, increasing the manufacturing costs. In addition, the time available for this study was limited. Thus, modification was rejected, leaving it out of scope.

5 Results and Discussion

The results of this work are presented, along this chapter, following the methods aforementioned. It has been divided in five sections: sensitive analysis, validation, optimal TSR, influence of inertia and new configurations.

All the results in this section have been compared with the reference simulation in which the turbine rotates at 1 rad/s. In order to familiarize the reader with the result, first the reference simulation, the results of this simulation are shown first.

In Figure 20, the velocity contours of the flow around the turbine in the plane parallel to the bottom of the channel can be observed. This figure consists on a sequence of six pictures along one full lap.

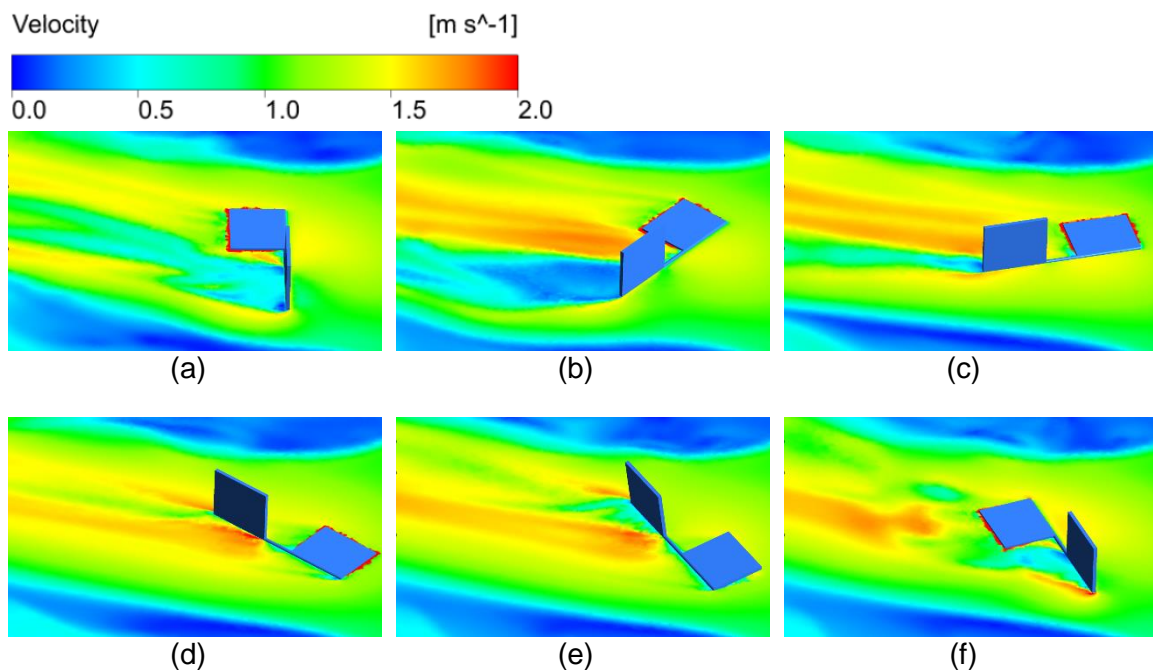


Figure 20. Sequence of one lap of the turbine represented with the velocity of the flow in the plane xz.

The flow facing the blades generates torque around “y” axis which is considered positive when it has the direction of the rotation (Figure 9). Thus, the torque extracted from the turbine will oscillate between positive and negative values. This oscillations on the torque can be seen in the following figure where the torque generated, and the pitch angle are shown.

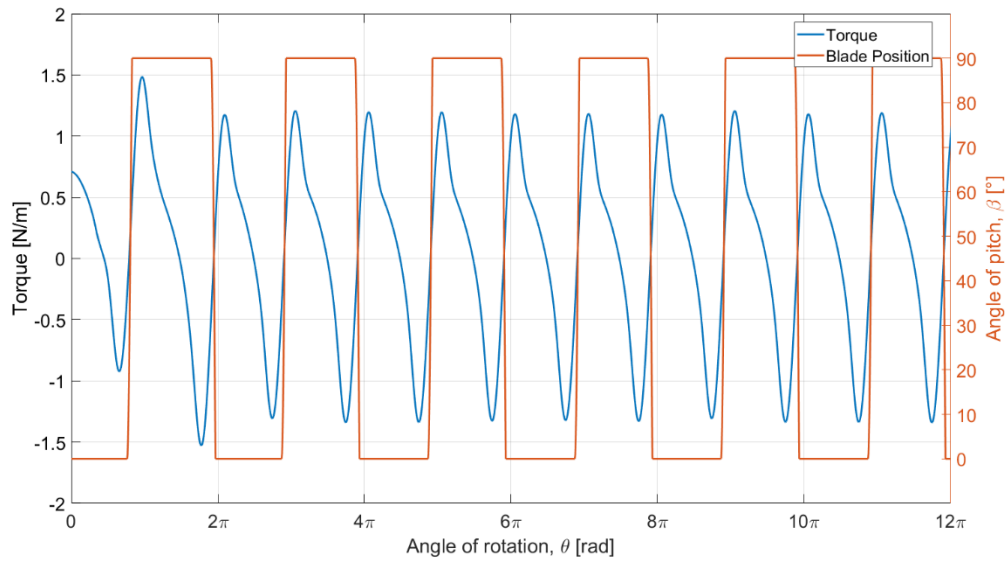


Figure 21. Torque extracted from the turbine and its pitch position along six laps.

The square wave corresponds to the pitch angle. When it changes from 0° to 90° (or the other way around) (Figure 20 (e) to (f)), the flow faces the blade in the positive sense. Hence the torque changes from negative to positive and increases until the face of the blade is perpendicular to the flow (Figure 20 (a)). In this point the torque is maximum. Then, the torque starts to decrease (Figure 20 (b) and (c)) and turns to the negative part (Figure 20 (d)) where the blade will remain in the negative part until the force is high enough to initiate the pitch (Figure 20 (e)).

As it was explained, the power and power coefficient can be easily calculated from the torque using equations (18) and (3). However, the results are based on the power coefficient and thus the torque is not used in their determination and, the C_p is calculated directly with equation (12).

5.1 Sensitive analysis

The results of the sensitive analysis are shown in Figure 22. Each point of the graph corresponds with the C_p obtained in each simulation with different degrees of mesh refinements. In Figure 22 is possible to observe the trend of the C_p which converges as the elements of the mesh increase.

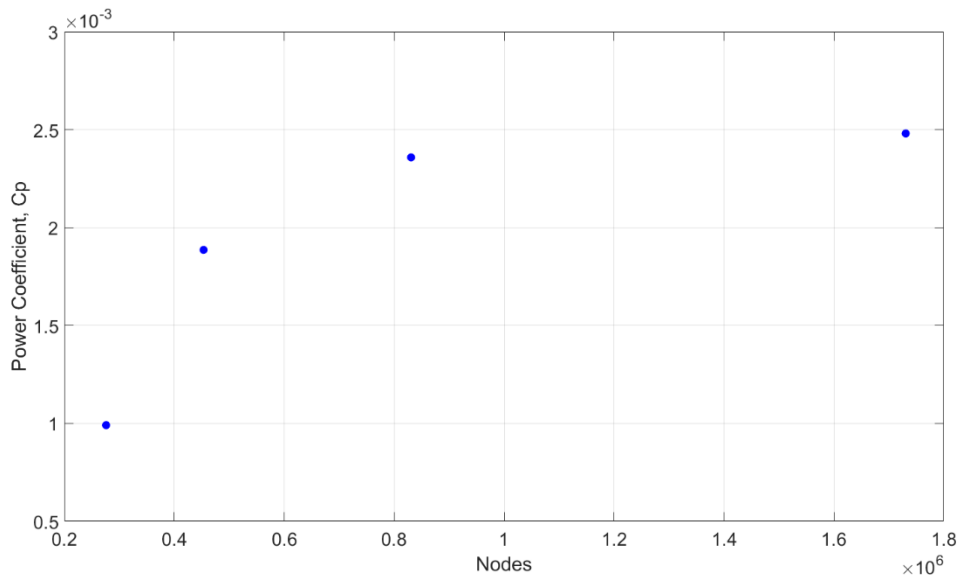


Figure 22. Sensitive analysis for the simulation rotating at 1 rad/s.

These differences are numerically expressed on Table 1 where the information of elements, C_p and relative error are gathered.

Table 1. Results of the sensitive analysis.

Simulation	Element	Power Coefficient	Relative Error [%]
1	2.76E+05	9.91E-04	47.57
2 (reference)	4.53E+05	1.89E-03	19.92
3	8.31E+05	2.36E-03	4.91
4	1.73E+06	2.48E-03	

It has been concluded that the optimal mesh is the one used in simulation number 3 because the error is lower than 5% as compared to the finest mesh. The latter has a considerably greater number of nodes than the other simulations. However, simulation 3 and 4 require a really high computational effort. For both cases five-day simulations with sixteen CPUS are not enough to complete seven laps of the turbine.

Hence mesh 2 was used. Although it has a significant error, it has been considered acceptable for these first stages of the design. Since many

simulations were needed and the time and the computational resources were limited.

5.2 Validation results

The validation process can be split in two parts as mentioned in the methodology. The first part refers to the calculation of “ β ” (the angle on the pitch, see Figure 19) and second the calculation of the C_p .

The analytical calculation of “ β ” based on equation (19), (20) and (21) is presented on the Figure 23. This calculation is presented together with the results provided by fluent, in order to compare both.

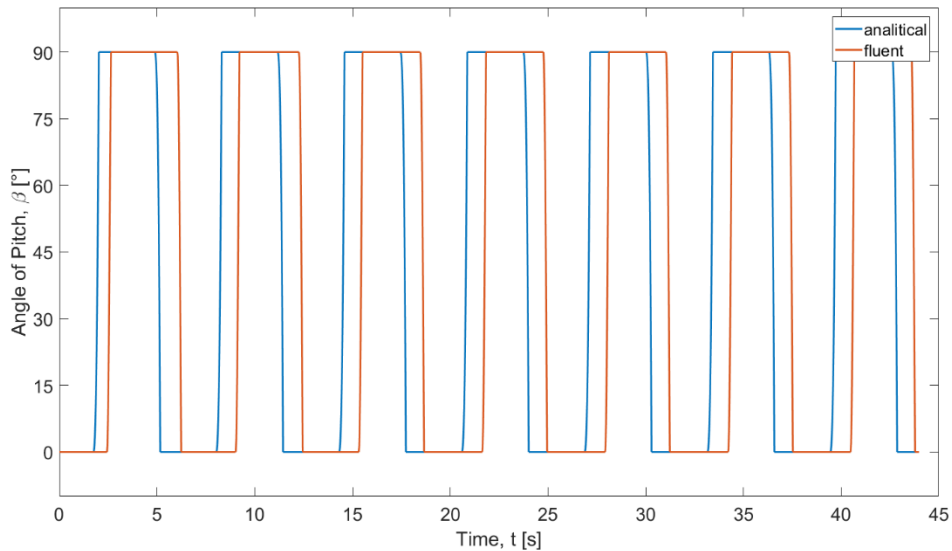


Figure 23. Comparison between the analytical results and the Ansys® Fluent v. 18.2 results of the angle of pitch.

According to the analytical model, the pitch is initiated 0.6 seconds earlier as compared to the predictions provided by the CFD model.

This result could be considered acceptable if the parameter had no effect on the calculations of the C_p . Being an intermediate result in the calculations, the error will be further accumulated, leading to a significant lack of accuracy of the model.

Results and Discussion

The earlier pitch motion in the analytical model is produced because the model just considers drag forces. In reality, there are more forces acting on the blade. This assumption results in an underestimation of the force acting on the blade. Less force in the blade means that the pitch force, i.e. the force in the opposite direction of the rotation appears earlier. This is shown in Figure 23.

However, the average C_p obtained with the analytical model is $2.58E-02$. This result is one order of magnitude greater than the obtained with fluent $2.48E-03$ (Table 1). It has been concluded that since the error of the pitch angle is quite high, this value is not accurate enough.

Hence before trying to develop a more complex analytical model, the pitch motion calculated by fluent was introduced in the analytical calculation of the C_p . As it shown in Figure 24, this result fits much better with the results of the simulations. In this case the mean value of the C_p is $4.2E-03$ which is about twice the value obtained in the simulation. The analytically calculated result can be considered an ideal value for this configuration of the turbine.

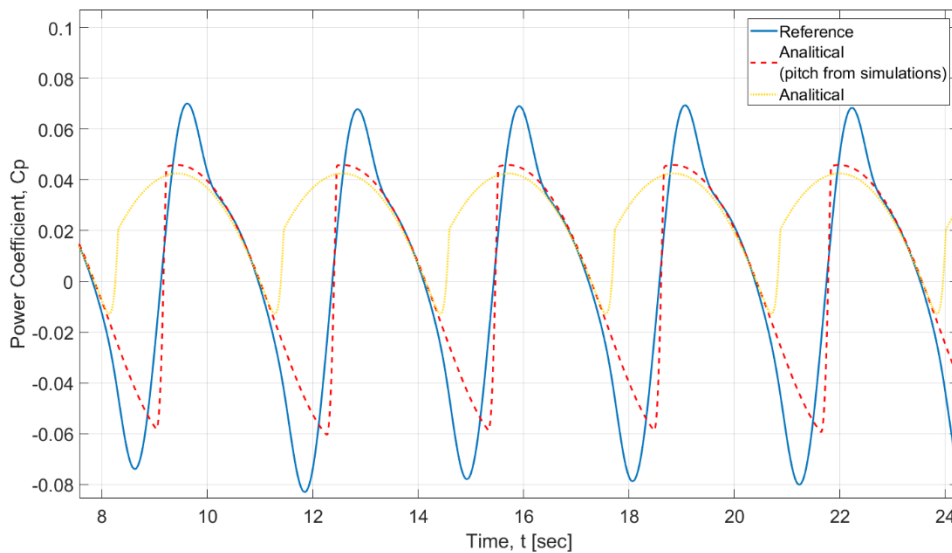


Figure 24. Comparison between the two-analytical approach and the reference simulation.

5.3 Optimal tip speed ratio

The optimal Tip Speed Ratio curve was calculated with four experimental points. They were adjusted to a second-degree polynomial curve, whose mathematical equation is in the legend together with the R^2 value.

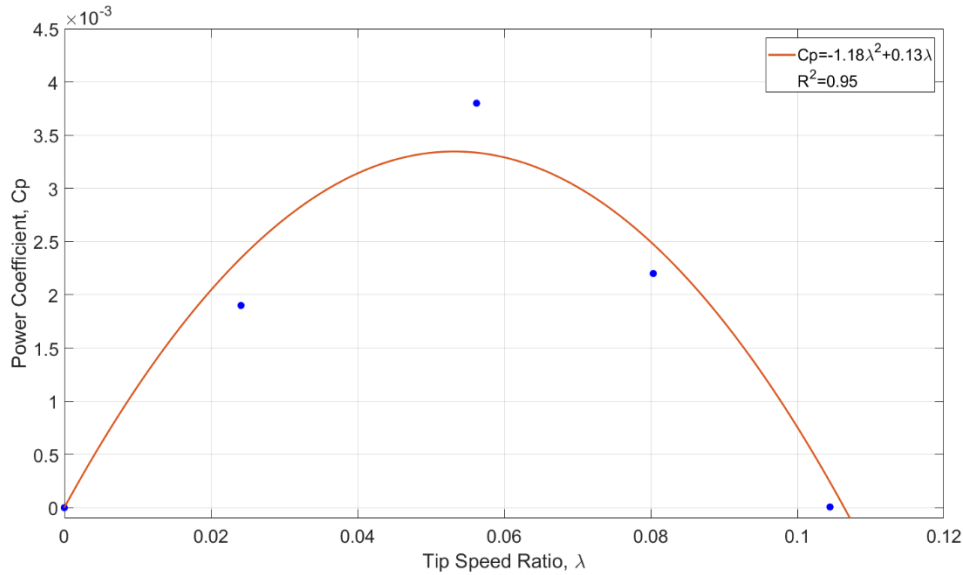


Figure 25. Power coefficient as function of the Tip Speed Ratio.

Thus, it is possible to calculate the optimal TSR by deriving the curve equation (22).

$$\frac{d}{d\lambda}(-1.18\lambda^2 + 0.13\lambda) = 0 \rightarrow -2.36\lambda + 0.13 = 0 \rightarrow \lambda = 0.055 \quad (22)$$

The optimal angular speed for the reference case can be calculated as follows:

$$\frac{w \cdot R}{U} = 0.055 \rightarrow w = 0.69 \frac{\text{rad}}{\text{s}} \rightarrow 6.5 \text{ rpm} \quad (23)$$

Under the optimal TSR conditions, a C_p of $3.58\text{E-}3$ is achieved. Although this velocity is rather low, it can be increased if the radius is reduced and if the turbine is placed in a zone where the flow is faster.

5.4 Influence of inertia around the shaft

The influence of the inertia on the power coefficient is shown in Figure 26. As the inertia decreases the power coefficient increases. The yellow line

Results and Discussion

corresponds to the real inertia of the geometry studied, which it could not be simulated due to the vibration produced explained in section 4.5.

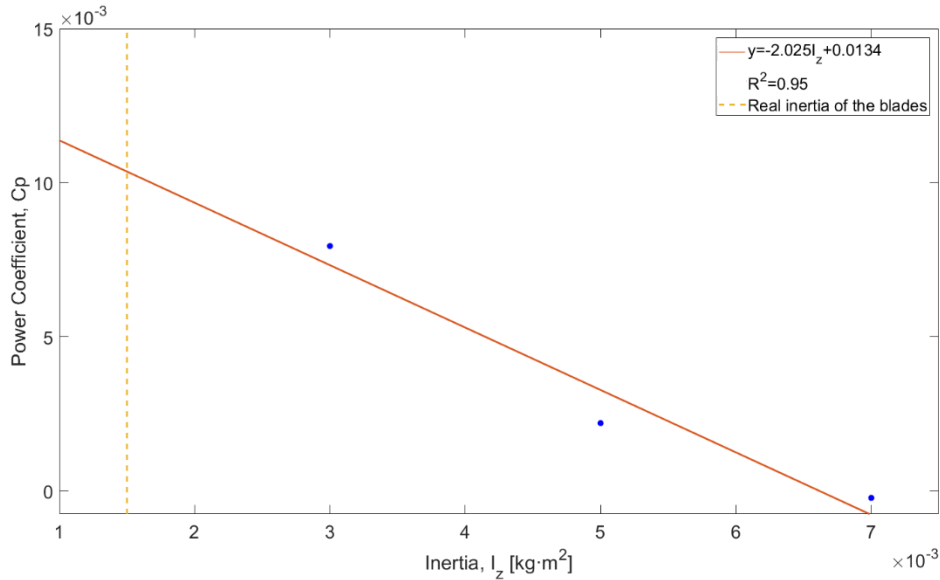


Figure 26. Influence of inertia on the average Power Coefficient.

The numerical data is gathered in Table 2. The regime of the turbine switches from consuming energy to producing it as the inertia is reduced. In fact, in the simulation with high inertia, the turbine does not produce any energy while in the reference simulation it is. Then from the reference simulation to the low inertia one the C_p increases by a factor of 3.6.

Table 2. Result from the inertia analysis.

Simulation	Inertia, I_z [kg·m ²]	Power Coefficient, C_p
High inertia	7E-3	-2E-4
Reference	5E-3	2.2E-03
Low Inertia	3E-3	7.9E-3

The trend of the previous graph has a R^2 of 0.95, which reflects being in good agreement with the data. It intersects the line of the real inertia with a C_p of 0.01 which is 4.7 times greater than the reference simulation.

According to equation (19) the angular acceleration of the pitch is directly proportional to the force on the blade and inversely proportional to the inertia. The force that produces the pitch is a force that contributes negatively to the generation of torque. Due to the rotation of the turbine, the slower the pitch motion, the greater the surface that faces the flow and the higher the force of the pitch, which contributes negatively to the torque.

Thus, this force should be kept as low as possible, to avoid worsening the performance of the turbine. Therefore, the pitch motion should be as fast as possible. It is evident that the greater the angular acceleration, the faster the pitch. By decreasing the inertia, high acceleration can be achieved in the pitch with low force, which results in an earlier initiation of the pitch.

This is also reflected in equation (24). In fact, the lower the inertia, the lower the energy necessary to move a body with a given angular speed.

$$E = \frac{1}{2} I_z \omega_z^2 \rightarrow \omega_z = \sqrt{\frac{2E}{I_z}} \quad (24)$$

In Figure 27, the first part of the graph shows the C_p during one complete lap. The low inertia simulation (orange) is the one in which negative C_p is minimized, therefore less energy was required to do the pitch. Also, it is the first one to achieve the maximum with the highest maximum of the three.

On the other hand, the simulation with high inertia has the lowest minimum and lowest maximum. On the second part of the figure the angle of pitch is represented. It can be observed that as the inertia is reduced the pitch is produced earlier.

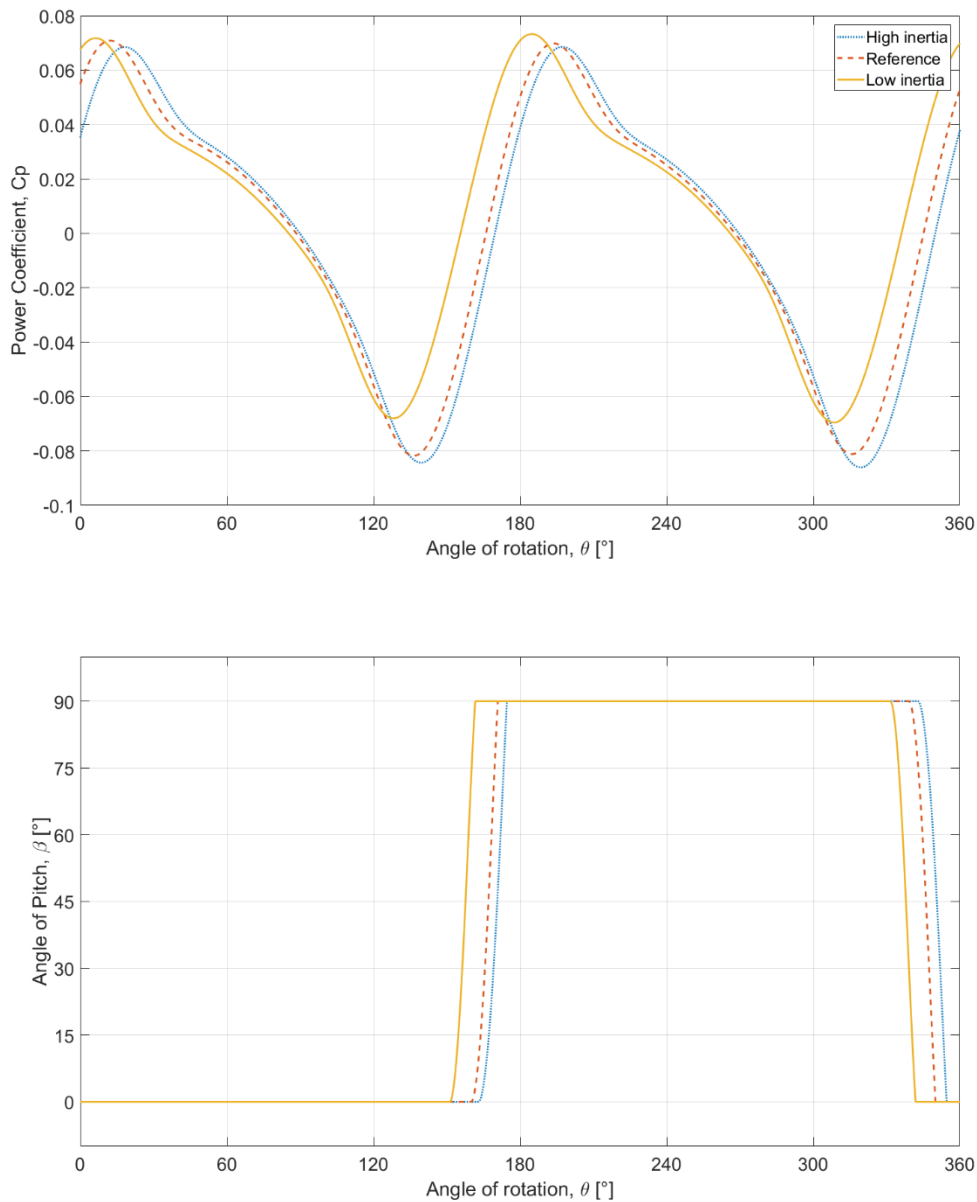


Figure 27. The effect of the inertia on: the C_p (figure on top) and on the angle of the pitch figure on the bottom. Both graphs are along one lap and during the same lap of the simulation, the fourth.

To conclude the inertia has been proven to be one of the main characteristic of the turbine proposed in this work. As it is capable of shifting the pitch to an earlier angle of rotation. 161.6°, 170.9 and 174.6 are the degrees where the pitch concludes for the simulations of low inertia, reference and high inertia respectively.

To summarize, the C_p is improved 3.6 times from the reference to the low inertia. Also, the C_p is expected to be increased by a factor of 4.7 with respect to the reference if simulations with the real inertia are carried out.

5.5 New configuration results

This work has considered some design improvements of the turbine in order to enhance its performance. One of these configurations consists on adding one pair of blades more. This is actually required since the model studied so far could act as a weather vane and not rotate.

5.5.1 Two pairs of blades

As aforementioned, the study of a turbine with four blades was a must. The same concept is maintained adding a pair of blades more which are shifted 90 degrees.

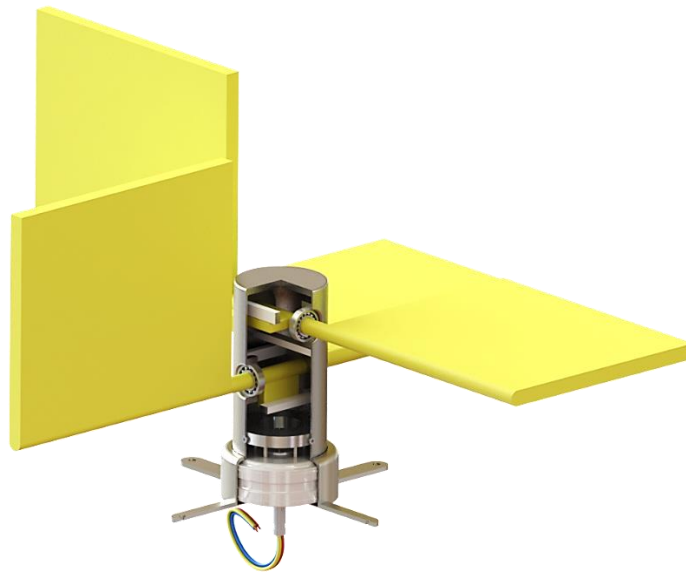


Figure 28. Two pair of blades configuration.

A smoother torque and consequently smoother and higher C_p is expected beforehand. The simulation set up is the same as the reference simulation but with one pair more of blades. In Figure 29 the torque generated by each pair of blades and its angle of pitch is shown. Also, the resultant torque produced by the turbine has been calculated.

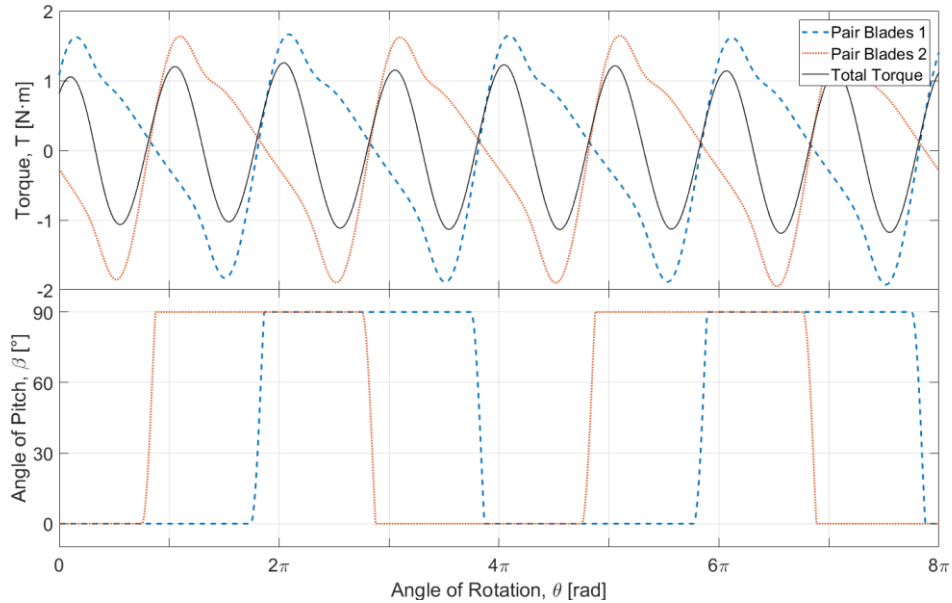


Figure 29. Pitch angle and torque generated by 2 pair of blades.

In the previous figure it is demonstrated that the resultant torque generated has lower maximums and minimums i.e. the torque is smoother. Basically, the torque does not fall to the negative part as much as with one pair of blades. Thanks to this the C_p increases to $5.1E-03$ which is 2.32 times greater than the reference value.

5.5.2 Four pairs of blades

Due to the good results obtained in the two pairs of blades simulations, simulating the turbine with more blades was required. If located in the same plane, the blades would hinder each other, thus adding two pair of blades more on top of the other two was considered. Hence there is a blade facing the flow perpendicularly every 45 degrees. In Figure 30 the arrangement of the turbine with four pair of blades is shown.

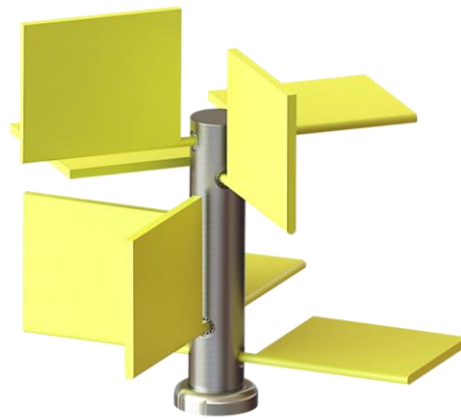


Figure 30. Design and arrangement of the turbine with four pairs of blades.

Beforehand, an increase of the power generated is expected beforehand. However, the C_p is uncertain since it depends on the projected area of the turbine which doubles in this arrangement.

Yet, the simulations have shown that the C_p increases as well. The result obtained is was $6.2E-03$ which is 3.8 times higher than the reference and 1.22 times higher than the previous case of two pair of blades.

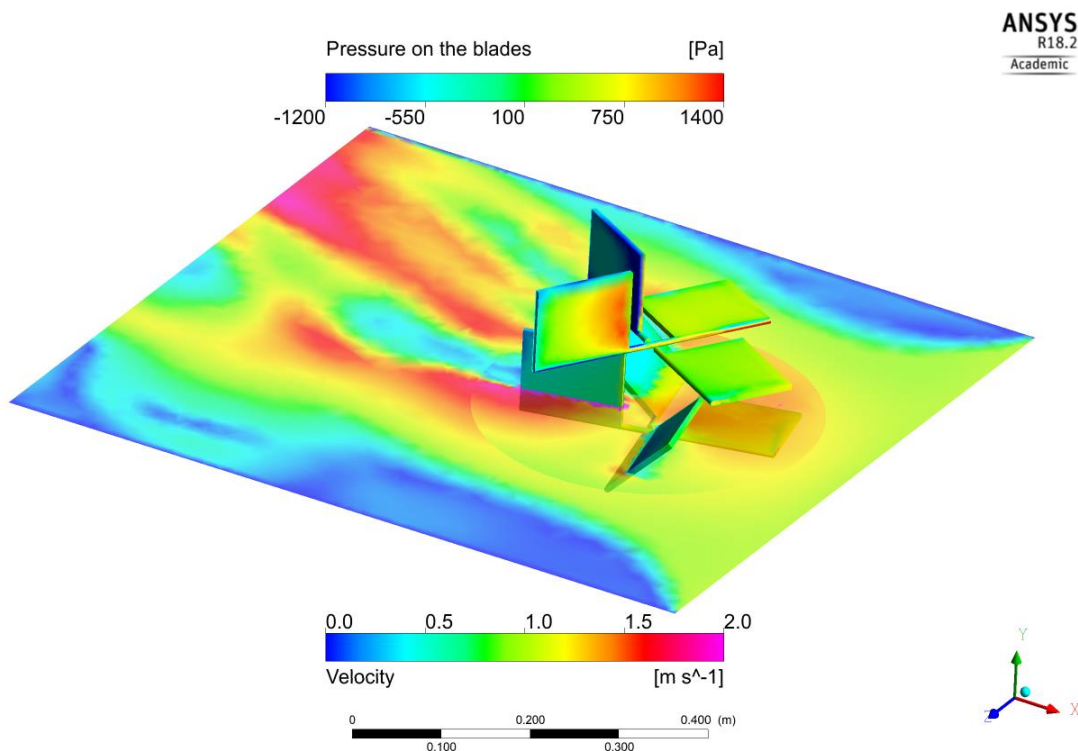


Figure 31. Four pair of blades colour contours from simulation.

The previous figure shows the result of the simulation where the pressure on the surface of the blades is coloured. Also, the contours of velocity are shown on the parallel plane to the bottom of the channel.

5.5.3 Shape of the of the blades

The shape studied in this work is a starting point. The geometry of the blades is one of the main things to modify in order to obtain better results. However, the study of the shape is quite wide, and a great amount of simulations would be needed if a consistent analysis is to be carried out. Hence this work focuses more in other parameters. However, an attempt to optimize the shape of the blades based on analytical model was made. Then the results obtained were compared with simulations.

First a code which runs the analytical model for different shapes was created. In Figure 32 the C_p achieved with different widths and heights blades is shown.

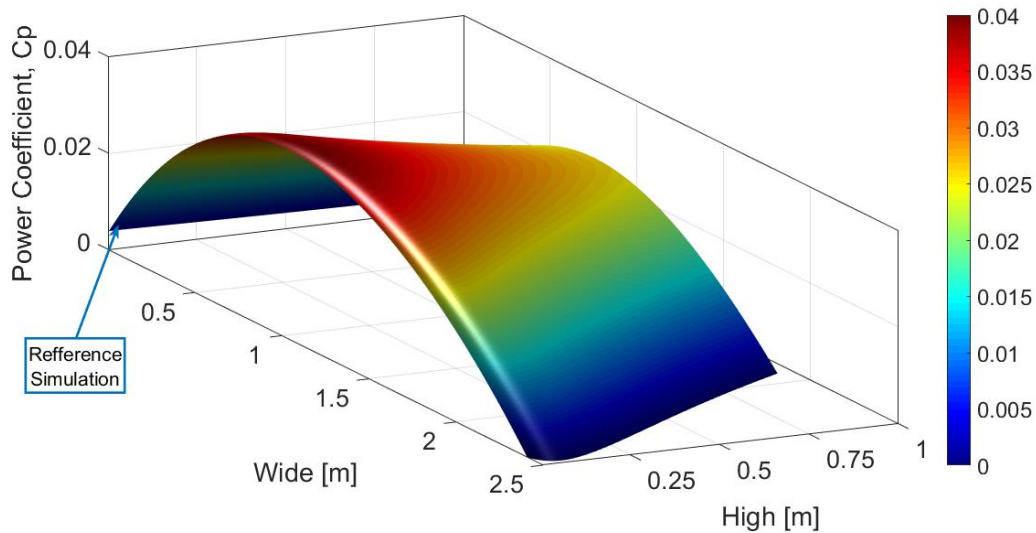


Figure 32. Optimization of the shape of blades with the analytical model.

The results of this optimization show that the maximum C_p is 0.04. Thus, the C_p can be incremented 6.9 times by changing the width and the height of the blades. In this analysis, the value of the thickness and the overblown of the inertia was held as in the reference simulation. The optimal geometry obtained is 1 meter of diameter and 0.1 meter of height. It resulted in a blade of 0.5x0.1

meters. This optimal shape is quite big for the simulations, since it is 3.4 times greater than the geometries simulated until now. Hence it was kept out of the scope of this thesis.

Note that this does not mean that the maximum diameter for this turbine is one meter. The maximum diameter which returns the optimal C_p for the particular shape of the blades used is one meter. However, there could be some other configurations that could increase the size, hence the power of the turbine.

6 Conclusions

The concept that the present work proposed, has been developed and assessed to the extent possible. The aims and objectives proposed have been satisfactorily fulfilled. The CFD model used has been validated through an analytical model and its convergence has been proved through a sensitive analysis.

Thus, from this thesis it can conclude that:

- **A CFD model was successfully developed, combining both sliding and dynamic mesh.** This model has shown a good convergence on its sensitive analysis. Besides the CFD model provides values of the C_p around 50% lower than the analytical model developed in all simulations. This overestimation obtained in the analytical model is due to the assumptions made.
- **The design was proven to be suitable for the generation of energy despite its simplicity.** The simulations performed confirm that even having low C_p ($2.48E-03$), the device proposed can generate energy. However, this low C_p can be attributed to the early stage in which the concept is. In fact, it has been shown that the C_p can be improved at least by 17.2 times by combining the decreasing of inertia, the addition of blades and the optimal speed.

A turbine in which the aforementioned improvements are combined would provide a C_p of $4.27E-02$. However, based on the predictions of the real inertia and the optimal shape the C_p could be increased up to $1.9E-01$. This value is slightly better than the C_p of a conventional Savounius rotor.

- **The design proposed is simple as far as the manufacturing process is concerned. In addition, it does not have an apparent impact on the river basin.** Due to its simplicity this turbine has big potential in the market. The manufacturing cost could be much lower than that of conventional turbines. This turbine could be implemented in locations where the electrification is not very developed, and the cost of self-supply

Conclusions

electricity is unaffordable. As it is common in rural areas of under developed and developing countries.

Besides, the turbine does not need any kind of barrier or channel. This increases the interest of this turbine as there is a growing concern for the production of clean sustainable power with low environmental impact from renewable energy sources.

7 Future work

As aforementioned, there are many different ways to improve the performance of the turbine since it is a rather immature concept. Thus, the future work regarding the design of the device is quite wide. In this section some guidelines are proposed.

The optimization of the shape of the turbine is one of the main challenges for the future. In fact, by changing the shape of the turbine the drag and the inertia change as well. It has been demonstrated that these parameters are the main parameters that governs the efficiency of the turbine.

Thus, for the geometry optimisation the following should be considered:

- To increase the area of the blade in order to maximise the force produced on the blade and consequently the torque and the power.
- To decrease the inertia around the shaft of the blades. as it was proved that would increase the C_p . This can be achieved by doing the blades lighter. Optimizing the thickness, manufacturing holes in the blade or splitting the blade in small blades are some of the possible solutions that would decrease the inertia effectively (Appendix B).
- To twist the blades in order to hold onto the positive torque after the pitch as more drag and lift forces would be added, resulting in a higher torque and power.

In the appendix it is possible to find the suggested designs mentioned in the above bullets points Appendix B.

Also, it would be interesting to study the effect of the velocity distribution of the flow. At the bottom of the water channels the velocity is zero and then it increases exponentially until it achieves the maximum velocity at the surface, Figure 12. Thus, when the arrangement of the turbine requires the blade to be located in different levels (i.e. when additional blades are introduced in the turbine), (Figure 30) the geometry of the blades should be optimised independently for each blade. The velocity of the flow that the blades face varies with the height in which they are located accordingly to the velocity profile

Future work

of the river. Therefore, if the performance of the turbine is to be optimised, the effect of the velocity distribution of the flow is a particularly relevant in certain configurations.

REFERENCES

- [1] G. Boyle, "Renewable energy," *Renew. Energy*, by Ed. by Godfrey Boyle, pp. 456. Oxford Univ. Press. May 2004. ISBN-10 0199261784. ISBN-13 9780199261789, p. 456, 2004.
- [2] A. A. Lahimer, M. A. Alghoul, K. Sopian, N. Amin, N. Asim, and M. I. Fadhel, "Research and development aspects of pico-hydro power," *Renew. Sustain. Energy Rev.*, vol. 16, no. 8, pp. 5861–5878, 2012.
- [3] R. L. Radkey and B. Hibbs, "Definition of cost-effective river-turbine designs," *NASA STI/Recon Tech. Rep. N*, vol. 83, 1981.
- [4] P. Garman, *Water Current Turbines. A Fieldworker's Guide*. Intermediate Technology Publications, 1986.
- [5] D. Powell, A. Ebrahimi, S. Nourbakhsh, M. Meshkaldini, and A. M. Bilton, "Design of pico-hydro turbine generator systems for self-powered electrochemical water disinfection devices," *Renew. Energy*, vol. 123, pp. 590–602, 2018.
- [6] P. Fraenkel, O. Parish, V. Bolkalders, A. Harvey, A. Brown, and R. Edwards, *Micro-hydro Power*. Practical Action Publishing, 1991.
- [7] The Open University, *Thermofluid Mechanics and Energy*. The Open University Press, 1982.
- [8] G. L. Wei *et al.*, "Impact of dam construction on water quality and water self-purification capacity of the Lancang River, China," *Water Resour. Manag.*, vol. 23, no. 9, pp. 1763–1780, 2009.
- [9] J. Zanette, D. Imbault, and A. Tourabi, "A design methodology for cross flow water turbines," *Renew. Energy*, vol. 35, no. 5, pp. 997–1009, 2010.
- [10] I. S. Hwang, Y. H. Lee, and S. J. Kim, "Optimization of cycloidal water turbine and the performance improvement by individual blade control," *Appl. Energy*, vol. 86, no. 9, pp. 1532–1540, 2009.

REFERENCES

- [11] K. Pope, I. Dincer, and G. F. Naterer, "Energy and exergy efficiency comparison of horizontal and vertical axis wind turbines," *Renew. Energy*, vol. 35, no. 9, pp. 2102–2113, 2010.
- [12] J. Melorose, R. Perroy, and S. Careas, "Wind Turbines: Fundamentals, Technology, Application, Economics," *Statew. Agric. L. Use Baseline 2015*, vol. 1, p. 897, 2015.
- [13] C. Garrett and P. Cummins, "Maximum power from a turbine farm in shallow water," *J. Fluid Mech.*, vol. 714, pp. 634–643, 2013.
- [14] G. A. M. Van Kuik, "The Lanchester-Betz-Joukowski limit," *Wind Energy*, vol. 10, no. 3, pp. 289–291, 2007.
- [15] P. B. S. Wilson, R.E.; Lissaman, *Applied Aerodynamics of Wind power Machines*. Oregon State University, 1974.
- [16] M. Hadi Ali, "Experimental Comparison Study for Savonius Wind Turbine of Two & Three Blades At Low Wind Speed," *Int. J. Mod. Eng. Res. www.ijmer.com*, vol. 3, no. 5, pp. 2978–2986, 2013.
- [17] K. Khavari, "Improvement in the efficiency of the Savonius rotor," Cranfield Institute of Tecnology. College of Aeronautics. Department of Aerodynamics, 1980.
- [18] H. J. Choi, M. A. Zullah, H. W. Roh, P. S. Ha, S. Y. Oh, and Y. H. Lee, "CFD validation of performance improvement of a 500 kW Francis turbine," *Renew. Energy*, vol. 54, pp. 111–123, 2013.
- [19] B. C. Cochran, D. Banks, and S. J. Taylor, "A Three-Tiered Approach for Designing and Evaluating Performance Characteristics of Novel WECS," *AIAA (American Inst. Aeronaut. Astronaut.*, no. January, p. 11, 2004.
- [20] S. McTavish, D. Feszty, and T. Sankar, "Steady and rotating computational fluid dynamics simulations of a novel vertical axis wind turbine for small-scale power generation," *Renew. Energy*, vol. 41, pp. 171–179, 2012.

REFERENCES

- [21] T. Kawamura, T. Hayashi, and K. Miyashita, "41. Application of the Domain Decomposition Method to the Flow around the Savonius Rotor," in *Domain Decomposition Methods in Sciences and Engineering*, 1998, p. 393.
- [22] T. Sankar and M. Tiryakioğlu, "Design and power characterization of a novel Vertical Axis Wind Energy Conversion system (VAWECS)," *Wind Eng.*, vol. 32, no. 6, pp. 559–572, 2008.
- [23] F. De Serio and M. Mossa, "Streamwise velocity profiles in coastal currents," *Environ. Fluid Mech.*, vol. 14, no. 4, pp. 895–918, 2014.
- [24] A. D. Canonsburg, "ANSYS Fluent Customization Manual," vol. 15317, no. January, pp. 724–746, 2015.
- [25] D.-L. and DrTakaNishino, "' CFD for Renewable Energy ' module – Tutorials FLUENT Tutorial 3 : Flow around a 1-bladed Vertical Axis Wind Turbine," no. December, pp. 1–16, 2017.
- [26] S. K. Carney, B. P. Bledsoe, and D. Gessler, "Representing the bed roughness of coarse-grained streams in computational fluid dynamics," *Earth Surf. Process. Landforms*, vol. 31, no. 6, pp. 736–749, 2006.
- [27] V. T. Nguyen and F. Nestmann, "Applications of CFD in Hydraulics and River Engineering," *Int. J. Comput. Fluid Dyn.*, vol. 18, no. 2, pp. 165–174, 2004.
- [28] M. Castro-García, J. I. Rojas-Sola, and E. De La Morena-de La Fuente, "Technical and functional analysis of Albolafia waterwheel (Cordoba, Spain): 3D modeling, computational-fluid dynamics simulation and finite-element analysis," *Energy Convers. Manag.*, vol. 92, pp. 207–214, 2015.
- [29] J. L. Menet, "A double-step Savonius rotor for local production of electricity: A design study," *Renew. Energy*, vol. 29, no. 11, pp. 1843–1862, 2004.
- [30] J. V. Akwa, H. A. Vielmo, and A. P. Petry, "A review on the performance

REFERENCES

- of Savonius wind turbines,” *Renew. Sustain. Energy Rev.*, vol. 16, no. 5, pp. 3054–3064, 2012.
- [31] K. Matsushima, M. Murayama, and K. Nakahashi, “Unstructured dynamic mesh for large movement and deformation,” *40th AIAA Aerosp. Sci. Meet. Exhib.*, no. January, 2002.
- [32] M. H. Patel, *Dynamics of Offshore Structures*: . Butterworth Heinemann, 2013.

APPENDICES

Appendix A Analytical Model

```
clear all
% rea data from fluent to compere
filename = 'Motion_pitch.out';
delimiterIn = ' ';
headerlinesIn = 5;
Motion_pitch_reff = importdata(filename,delimiterIn,headerlinesIn);
pitch_reff=Motion_pitch_reff.data(:,7);
time2=Motion_pitch_reff.data(:,1);

filename = 'cm-rfile.out';
delimiterIn = ' ';
headerlinesIn = 3;
reff_cm_file = importdata(filename,delimiterIn,headerlinesIn);

time_step=reff_cm_file.data(:,1);
cm_reff=-reff_cm_file.data(:,2);
cm_reff_smooth =smooth(time_step,cm_reff,0.08,'loess');

%% Analitical
%geometry
high=0.1035;%m
width_b=0.12;%m
width=0.3;%m
area=width*high; %m2
area_b=high*width_b;
diameter_s=0.007;
area_shaft=diameter_s*width/2;
Cd=1.6;
Cd_shaft=0.295;
added_coef=0.6151;
radius=(width_b/2)+(width-width_b*2)/2; %m 0.09
density_mat= 2700; %kg/m3 aluminiun
inertia=0.005;%density_mat*diameter_s*high*width*high^2*1/4;%
%simulation data
w=1; %rads/s
step=0.0008/w; %time step
steps=54978;
density=998.2; %kg/m3
U=1.1211; %m/s velocity fluid
%initial values
pitch_pos=1;
acel_ang=0;
time=0;
beta=zeros(steps+1,1); %angle of the blade
blad1=zeros(steps,1);
blade2=zeros(steps,1);
```

```

vel1=zeros(steps,1);
vel2=zeros(steps,1);
k1=sign(vel1);
k2=sign(vel2);
Fd1=zeros(steps,1);
F11=zeros(steps,1);
F1=zeros(steps,1);
Fd2=zeros(steps,1);
F12=zeros(steps,1);

F2=zeros(steps,1);
theta=zeros(steps,1);
w_b=zeros(steps+1,1);% vel of the pitch

for

    l=1:1:steps
    time=step*l;
    theta(l+1)=w*time;

%     Cd=abs(2.*(sin(theta(l+1)+pi/2)).^2);
%     Cl=abs(sin(2*(theta(l+1)))));

    blade1(l)=cos(beta(l));
    blade2(l)=sin(beta(l));

    vel1(l)=U-w*radius*(cos(theta(l+1)));
    vel2(l)=U-w*radius*(cos(theta(l+1)-pi));

    Fd1(l)=0.5*density*vel1(l)^2*Cd*area_b-
    0.5*density*vel2(l)^2*Cd_shaft*area_shaft;

%     F11(l)=0.5*density*vel1(l)^2*Cl*area_b;
    F1(l)=sqrt(Fd1(l)^2+F11(l)^2)*blade1(l);
    F1(l)=F1(l)*(cos(theta(l+1)));

    Fd2(l)=0.5*density*vel2(l)^2*Cd*area_b-
    0.5*density*vel1(l)^2*Cd_shaft*area_shaft;

%     F12(l)=0.5*density*vel2(l)^2*Cl*area_b;
    F2(l)=sqrt(Fd2(l)^2+F12(l)^2)*blade2(l);
    F2(l)=F2(l)*(cos(theta(l+1)+pi));

    gravity_f=density_mat*diameter_s*area_b*9.81;

    if F1(l)<-gravity_f*cos(beta(l)) && pitch_pos==1

        added_mass_force=2*density*added_coef*diameter_s*high*width_b*ace
l_ang*(high/2);

        acel_ang=(high/2)*(-F1(l)+F2(l)+gravity_f*sin(beta(l))-
added_mass_force)/inertia;

```

```

w_b(l+1)=w_b(l)+acel_ang*step;
beta(l+1)=beta(l)+w_b(l+1)*step+(acel_ang*step^2)/2;
if beta(l+1)>(pi/2)
    beta(l+1)=pi/2;
    w_b(l+1)=0;
    pitch_pos=0;

end

elseif pitch_pos==1
    beta(l+1)=0;

end

if pitch_pos==0 && F2(l)>0
    beta(l+1)=pi/2;
end

if F2(l)<-gravity_f*sin(beta(l)) && pitch_pos==0
added_mass_force=2*density*added_coef*diameter_s*high*width_b*acel_ang*
(high/2);

acel_ang=(high/2)*(F1(l)+-F2(l)+gravity_f*cos(beta(l))-added_mass_force)

w_b(l+1)=w_b(l)-acel_ang*step;
beta(l+1)=beta(l)+w_b(l+1)*step-(acel_ang*step^2)/2;
if beta(l+1)<0.00001
    beta(l+1)=0;
    w_b(l+1)=0;
    pitch_pos=1;

end

elseif pitch_pos==0
    beta(l+1)=pi/2;
end

end

M=radius*(F1+F2);
P=M*w;
Cp_analitical=P*(0.5*density*area*U^3).^-1;

Cp=mean(Cp_analitical)

```

Appendix B Suggested designs

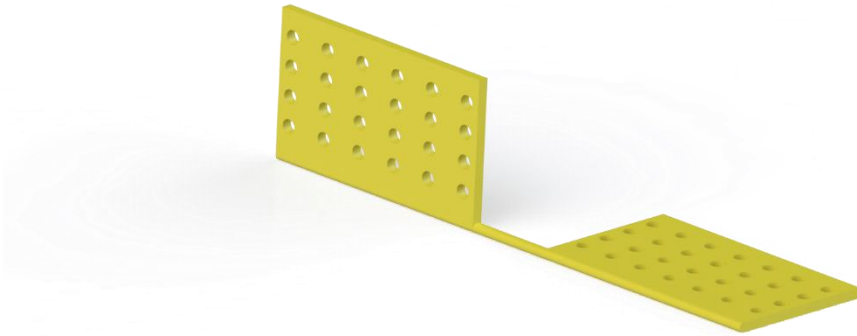


Figure 33. Holes manufactured on the blades in order to reduce the inertia.

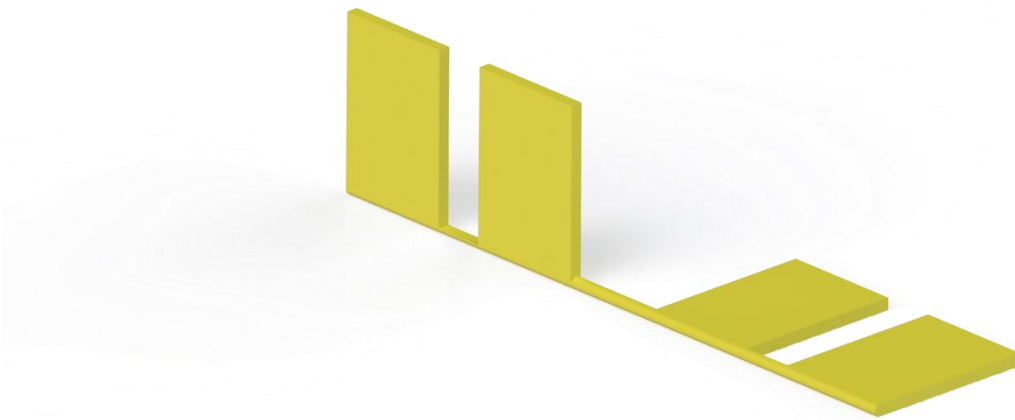


Figure 34. Blades split in different plates in order to reduce the inertia.

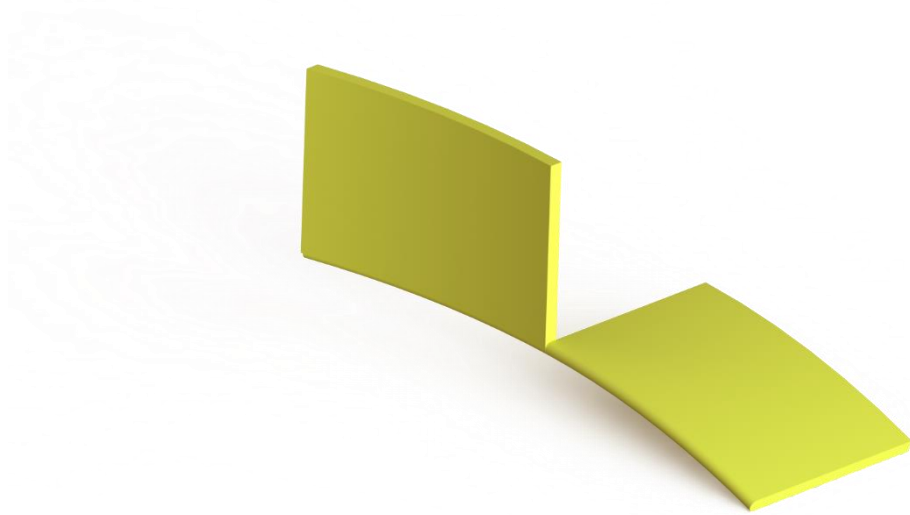


Figure 35. Twisted blades in order to increase the force on the blades.